Analysis of Variants Within the Porous Media Transport Models

B. Alazmi

K. Vafai
e-mail: Vafai.1@osu.edu

Department of Mechanical Engineering,
The Ohio State University,
Columbus, OH 43210

An investigation of variants within the porous media transport models is presented in this work. Four major categories in modeling the transport processes through porous media, namely constant porosity, variable porosity, thermal dispersion, and local thermal nonequilibrium, are analyzed in detail. The main objective of the current study is to compare these variances in models for each of the four categories and establish conditions leading to convergence or divergence among different models. To analyze the effects of variants within these transport models, a systematic reduction and sensitivity investigation for each of these four aspects is presented. The effects of the Darcy number, inertia parameter, Reynolds number, porosity, particle diameter, and the fluid-to-solid conductivity ratio on the variances within each of the four areas are analyzed. It is shown that for some cases the variances within different models have a negligible effect on the results while for some cases the variations can become significant. In general, the variances have a more pronounced effect on the velocity field and a substantially smaller effect on the temperature field and Nusselt number distribution. [S0022-1481(00)02602-5]

Keywords: Convection, Heat Transfer, Modeling, Porous Media

1 Introduction

Modeling of the non-Darcian transport through porous media has been the subject of various recent studies due to the increasing need for a better understanding of the associated transport processes. This interest stems from the numerous practical applications which can be modeled or can be approximated as transport through porous media such as thermal insulation, packed bed heat exchangers, drying technology, catalytic reactors, petroleum industries, geothermal systems, and electronic cooling. The work of Vafai and Tien [1] presented and characterized the boundary and inertial effects in forced convective flow through a porous medium. Later, Vafai and Tien [2] investigated the boundary and inertial effects on convective mass transfer in porous media. Vafai and Kim [3] used the Brinkman-Forcheimer-extended Darcy model to obtain a closed-form analytical solution for fully developed flow in a porous channel subject to constant heat flux boundary conditions. Hadim [4] performed a numerical study to analyze steady forced convection in a channel filled or partially filled with a porous medium and containing discrete heat sources. Kaviany [5] studied the flow through a constant porosity medium bounded by isothermal parallel plates using the Brinkman-extended flow model and constant matrix porosity. Lauriat and Vafai [6] presented a comprehensive study of forced convective heat transfer in porous media through a channel or over a flat plate.

Other research works consider various problems of the flow and heat transfer through a constant porosity medium (Beckerman and Viskanta [7], Kim and Choi [8], Kladias and Prasad [9], Nield et al. [10], Sung et al. [11], You and Chang [12,13], Neale and Nader [14], Poulikakos and Kazmierczak [15], Kim et al. [16], Chen and Vafai [17], Nakayama et al. [18], Hong et al. [19], Kaviany [20], Kuznetsov [21], Lan and Khodadadi [22], Nakayama et al. [23], Ould-Amer et al. [24], Vafai and Kim [25,26]). A synthesis of various aspects of modeling of transport processes in porous media was given in Tien and Vafai [27]. Recent monographs in which some aspects of transport in porous media were discussed have been presented by Kaviany [28] and Nield and Bejan [29].

A number of experimental and theoretical studies have shown that variation of porosity near a solid boundary has a significant effect on the velocity fields in packed beds resulting in an appreciable flow maldistribution, which appears as a sharp peak near the solid boundary and decreases to nearly a constant value at the center of the bed. This phenomenon is known as the channeling effect. Vafai [30,31] and Vafai et al. [32] investigated analytically and experimentally the channeling effect on an external forced convective flow and heat transfer. Poulikakos and Renken [33] presented a numerical study of the variable porosity effects in a channel bounded by two isothermal parallel plates and in a circular pipe. A number of investigations have considered the effect of variable porosity on fluid flow and heat transfer in porous media (Renken and Poulikakos [34], Hunt and Tien [35,36], and Hsiao et al. [37]).

It is well documented in the literature that the effect of thermal dispersion is essential for a number of applications in the transport processes through porous media. As such, a number of investigations have considered the effects of both thermal dispersion and variable porosity (Hunt and Tien [35,36], Hsiao et al. [37], Hong et al. [38], Chen [39–41], David et al. [42], Hsu and Cheng [43], Cheng et al. [44], Fu et al. [45], and Chen et al. [46]). On the other hand, some other investigations considered only the effect of thermal dispersion (Jang and Chen [47], Hunt and Tien [35,36], and Hong and Tien [48]). Cheng and Hsu [49] analyzed the wall effect of the thermal dispersion process in the forced convective flow through an annular packed-sphere bed. Cheng and Zhu [50] studied the effects of radial thermal dispersion on fully developed forced convection in cylindrical packed tubes. Later, Cheng and Vortemeyer [51] studied the effect of transverse thermal dispersion on fully developed forced convection in packed beds. Vafai and Amiri [52] have shown that the effect of longitudinal dispersion is insignificant for $Pe>10$. Their results show that the effect of transverse dispersion is much more important than the longitudinal dispersion.

The assumption of local thermal equilibrium (LTE) is widely used in analyzing transport processes through porous media. However, this assumption is not valid for some applications where a substantial temperature difference exists between the solid phase and the fluid phase. Amiri and Vafai [53] and Amiri et al. [54] employed a fully general model for the momentum equation and a two-phase model for the energy equation, including axial and transverse thermal dispersion to investigate forced convection in a channel. They presented detailed error maps for assessing the importance of various simplifying assumptions that are commonly used. In addition, Amiri and Vafai [55] presented a comprehensive numerical study for the problem of transient incompressible

Contributed by the Heat Transfer Division for publication in the JOURNAL OF HEAT TRANSFER. Manuscript received by the Heat Transfer Division, Sept. 30, 1999; revision received, Dec. 16, 1999. Associate Technical Editor: J. Howell.

flow through a packed bed including inertia and boundary effects in the momentum equation and the effects of thermal dispersion and local thermal nonequilibrium (LTNE) in the energy equation. Hwang et al. [56] investigated the non-Darcian forced convection taking into account the effects of boundary, inertia, and transverse thermal dispersion. Dixon and Cresswell [57] investigated the problem of LTNE between the fluid and solid phases and obtained a correlation for the fluid-to-solid heat transfer coefficients. Kuznetsov [58] presented an analytical solution for the simplified version of LTNE in a parallel plate channel subject to constant heat flux boundary conditions.

Four major categories in modeling the transport processes through porous media are analyzed in detail in this work. These four categories are related to transport aspects for constant porosity, variable porosity, thermal dispersion, and LTNE. As such, many different pertinent research works are systematically analyzed in the present investigation. For each category, a number of research works are found to be relevant to the present investigation. In all the above-mentioned investigations, variants of Darcy, Forchheimer, and Brinkman terms in the momentum equation as well as variants of thermal dispersion terms and the LTNE presentations were utilized. The main objective of the present work is to investigate and compare variances in models for each of the four categories and establish conditions leading to convergence or divergence among different models.

2 Problem Formulation

To analyze the four major categories in modeling the transport processes through porous media, a fundamental configuration shown in Fig. 1 is selected. This configuration consists of a parallel plate channel with constant heat flux q_w or constant wall temperature T_w. The height and the width of the channel are $2H$ and L, respectively. The velocity of the upstream flow is u_c and its temperature is T_e. This configuration allows an investigation of all the major aspects described earlier. The main assumptions for this investigation are summarized as follows:

1 The flow is steady and incompressible.
2 The properties of the porous medium and the fluid are isotropic and homogeneous.
3 The thermophysical properties of the fluid and the porous matrix are assumed to be constant.
4 Only the effect of transverse thermal dispersion is included, i.e., the effect of longitudinal dispersion is neglected. This is justified in light of the analysis by Amiri and Vafai [53].

The governing equations for the present investigation assuming fully developed conditions, can be written as given in Vafai [30], Vafai and Kim [3], and Amiri and Vafai [53]:

(a) Momentum Equation.

$$\frac{\rho_f}{\varepsilon}\langle (V\cdot\nabla)V\rangle = -\frac{\mu}{K}\langle V\rangle - \frac{\rho_f F\varepsilon}{\sqrt{K}}[\langle V\rangle\cdot\langle V\rangle]J + \frac{\mu}{\varepsilon}\nabla^2\langle V\rangle - \nabla\langle P\rangle \tag{1}$$

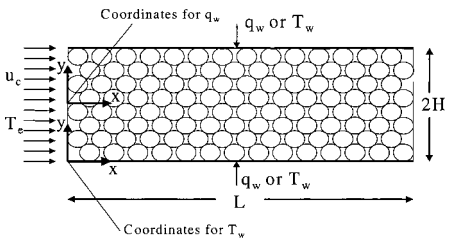

Fig. 1 Schematic diagram of the problem and the corresponding coordinate systems

For variable porosity case, the permeability of the porous medium K and the geometric function F can be represented as in Ergun [59] and Vafai [30,31]:

$$K = \frac{\varepsilon^3 d_P^2}{150(1-\varepsilon)^2} \tag{2}$$

$$F = \frac{1.75}{\sqrt{150\varepsilon^3}} \tag{3}$$

According to Benenati and Brosilow [60] and Vafai [30,31], the porosity distribution throughout the porous medium can be presented by the following equation:

$$\varepsilon = \varepsilon_\infty\left[1 + b\exp\left(\frac{-cy}{d_p}\right)\right]. \tag{4}$$

(b) Energy Equation.

$$(\rho C_P)_f\langle V\rangle\cdot\nabla\langle T\rangle = \nabla\cdot\left[\frac{k_{\text{eff}}}{\varepsilon}\cdot\nabla\langle T\rangle\right] \tag{5}$$

For thermal dispersion (Amiri and Vafai [53] and Amiri et al. [54])

$$k_{\text{eff}} = k_o + k_d \tag{6}$$

where k_o is the stagnant thermal conductivity and k_d is the dispersion conductivity.

For LTNE, two separate energy equations are required (Vafai and Amiri [52], Amiri and Vafai [53], and Amiri et al. [54]):

Fluid-Phase Energy Equation.

$$(\rho C_P)_f\langle V\rangle\cdot\nabla\langle T_f\rangle = \nabla\cdot\{k_{f\,\text{eff}}\cdot\nabla\langle T_f\rangle\} + h_{sf}a_{sf}(\langle T_s\rangle - \langle T_f\rangle) \tag{7}$$

Solid-Phase Energy Equation.

$$0 = \nabla\cdot\{k_{s\,\text{eff}}\cdot\nabla\langle T_s\rangle\} - h_{sf}a_{sf}(\langle T_s\rangle - \langle T_f\rangle) \tag{8}$$

where

$$k_{f\,\text{eff}} = \varepsilon k_f \tag{9}$$

and

$$k_{s\,\text{eff}} = (1-\varepsilon)k_s\,. \tag{10}$$

3 Problem Setup and Validation

An implicit method was used to solve the fully developed velocity field. The nonlinear term (Forchheimer term) was linearized by using the prior iteration values of the velocity. Convergence was considered to have been achieved when the absolute error between two successive iterations was less than 10^{-6}. The successive over relaxation method (SOR) was used to accelerate the convergence rate. The energy equation was solved by applying a central differencing for the diffusion term and upwind differencing for the convection term.

Numerical investigations were performed using different number of grid points to assess and ascertain grid independence results for the field variables. It was found that any increase beyond a set given by 500×1000 results in less than 0.2 percent change in the results. The local Nusselt number distribution was found using a three point differencing. Due to symmetry considerations, the solution is found for the upper half of the channel for the constant porosity category and for the lower half of the channel for the other three categories.

4 Results and Discussion

The numerical results for the constant porosity category were compared with the exact solution given by Vafai and Kim [3] as shown in Fig. 2, and an excellent agreement was found. The accuracy of the simulation of the variable porosity effects were

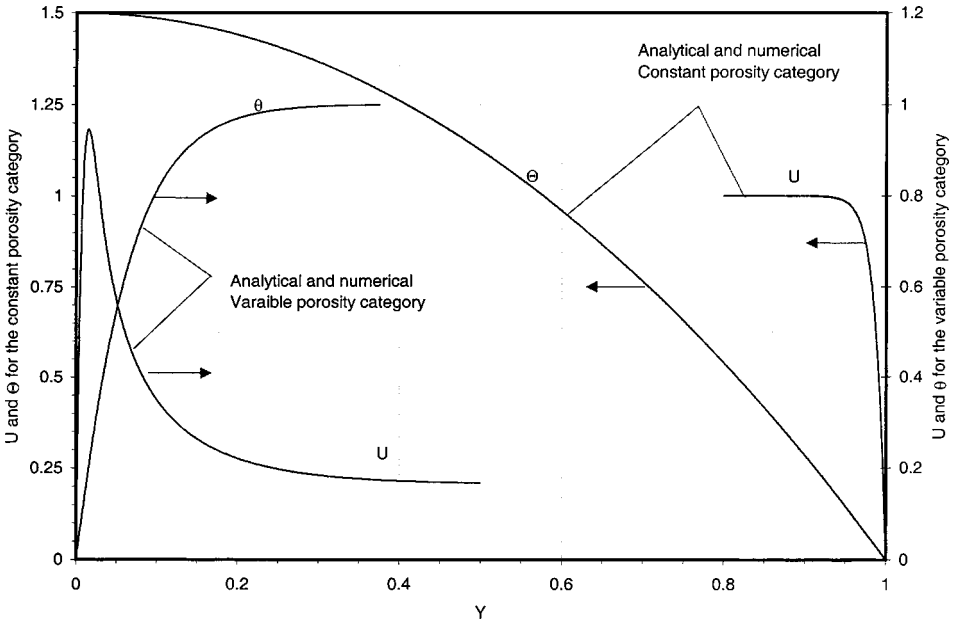

Fig. 2 Comparisons between the numerical results of the present study and the analytical solutions of Vafai and Kim [3] and Vafai [30]. The constant porosity category [$\varepsilon=0.9$, $\Lambda=100$, Da=0.001 and Re=100]. The variable porosity category [$dp/dx=-1493$, $d_p=0.008$, $b=0.98$, $c=2.0$, and $\varepsilon_\infty=0.5$].

checked against the analytical solution given in Vafai [30] and are presented in Fig. 2. An excellent agreement was found between the numerical results and the analytical solution given in Vafai [30]. In what follows, the results for each category are presented separately. Figure 1 describes the coordinate system and schematic of the fundamental configuration for the case of constant porosity as well as the fundamental configuration for the other

Table 1 Relationship between various models and the pertinent literature

Model	References
C1	Vafai and Tien [1,2], Vafai and Kim [3], Kaviany [5], Lauriat and Vafai [6], Hong et al. [19], Kaviany [20], Kuznetsov [21], Lan and Khodadadi [22], Nakayama et al. [23], Ould-Amer et al. [24], Vafai and Kim [25,26]
C2	Kim et al. [16], Chen and Vafai [17], Nakayama et al. [18]
C3	Hadim [4], Beckermann and Viskanta [7], Kim and Choi [8], Kladias and Prasad [9], Nield et al. [10], Sung et al. [11], You and Chang [12,13], Neale and Nader [14], Poulikakos and Kazmierczak [15]
V1	Vafai [30], Vafai [31], Vafai et al. [32], Vafai and Amiri [52], Amiri and Vafai [53], Amiri et al. [54], Amiri and Vafai [55]
V2	Lauriat and Vafai [6], Poulikakos and Renken [33], Renken and Poulikakos [34]
V3	Hunt and Tien [36], Hong et al. [38], Chen [39–41], Cheng et al. [44], Chen et al. [46]
V4	Hsiao et al. [37], David et al. [42], Hsu and Cheng [43], Fu et al. [45]
D1	Hong et al. [38], Hong and Tien [48], Vafai and Amiri [52], Amiri and Vafai [53], Amiri et al. [54], Amiri and Vafai [55]
D2	Chen [39–41], David et al. [42], Hsu and Cheng [43], Jang and Chen [47]
D3	Hsu and Cheng [43], Cheng et al. [44], Fu et al. [45], Vafai and Amiri [52], Hwang et al. [56]
D4	Chen et al. [46]
D5	Hunt and Tien [35,36]
E1	Vafai and Amiri [52], Amiri and Vafai [53], Amiri et al. [54], Amiri and Vafai [55]
E2	Hwang et al. [56]
E3	Dixon and Cresswell [57]

Table 2 Different models of constant porosity

Model	Darcy	Forchheimer	Brinkman
C1**	$\frac{\mu}{K}u$	$\rho\frac{F\varepsilon}{\sqrt{K}}u^2$	$\frac{\mu}{\varepsilon}\nabla^2 u$
C2	$\frac{\mu}{K}u$	$\rho\frac{F}{\sqrt{K}}u^2$	$\frac{\mu}{\varepsilon}\nabla^2 u$
C3*	$\frac{\mu}{K}u$	$\rho\frac{F}{\sqrt{K}}u^2$	$\mu\nabla^2 u$

*References [14] and [15] did not include the Forchheimer term. In comparisons, to properly concentrate on the difference with other models, a Forchheimer term was used within each of the categories.
**This model was used in the exact solution of Vafai and Kim [3].

Table 3 Different models of variable porosity (modified models)

Model	Darcy	Forchheimer	Brinkman
V1	$\mu\frac{150(1-\varepsilon)^2}{\varepsilon^3 d_p^2}u$	$\rho\frac{1.75(1-\varepsilon)}{\varepsilon^2 d_p}u^2$	$\frac{\mu}{\varepsilon}\nabla^2 u$
V2*	$\mu\frac{150(1-\varepsilon)^2}{\varepsilon^3 d_p^2}u$	$\rho\frac{1.75(1-\varepsilon)}{\varepsilon^3 d_p}u^2$	$\mu\nabla^2 u$
V3*	$\mu\frac{150(1-\varepsilon)^2}{\varepsilon^3 d_p^2}u$	$\rho\frac{1.75(1-\varepsilon)}{\varepsilon^3 d_p}u^2$	$\frac{\mu}{\varepsilon}\nabla^2 u$
V4	$\mu\frac{150(1-\varepsilon)^2}{\varepsilon^2 d_p^2}u$	$\rho\frac{1.75(1-\varepsilon)}{\varepsilon^2 d_p}u^2$	$\mu\nabla^2 u$

*In these models, the Darcy's term constant was changed from 175 into 150 for the purpose of comparison.

Table 4 Different models of transverse thermal dispersion

Model	Dispersion Conductivity	Notes
D1	$\gamma\rho C_P U d_p$	$\gamma=0.1$ $\gamma=0.2$
D2	$\gamma\frac{1-\varepsilon}{\varepsilon}\rho C_p U d_p$	$\gamma=0.04$ $\gamma=0.02$
D3	$\gamma\rho C_P U d_p\left(1-\exp\left(\frac{-y}{wH}\right)\right)$	$\gamma=0.17$, w=1.5 $\gamma=0.12$, w=1.0 $\gamma=0.3$, w=3.5 $\gamma=0.375$, w=1.5
D4	$0.01\frac{1-\varepsilon}{\varepsilon^2}\rho C_P U d_p$	
D5	$0.025\rho C_P U\sqrt{K}$	

Table 5 Different models of the fluid to solid heat transfer coefficient and the fluid to solid specific area

Model	h_{sf}	a_{sf}	Notes
E1	$\frac{k_f(2+1.1\mathrm{Pr}^{1/3}\mathrm{Re}^{0.6})}{d_p}$	$\frac{6(1-\varepsilon)}{d_p}$	
E2	$0.004\left(\frac{d_V}{d_p}\right)\left(\frac{k_f}{d_p}\right)\mathrm{Pr}^{0.33}\mathrm{Re}^{1.35}$	$\frac{20.346(1-\varepsilon)\varepsilon^2}{d_p}$	Re<75
	$1.064\left(\frac{k_f}{d_p}\right)\mathrm{Pr}^{0.33}\mathrm{Re}^{0.59}$		Re>350
E3*	$\left[\frac{d_p\varepsilon}{0.2555\mathrm{Pr}^{1/3}\mathrm{Re}^{2/3}k_f}+\frac{d_p}{10k_s}\right]^{-1}$	$\frac{6(1-\varepsilon)}{d_p}$	

*In this model, a_{sf} was taken similar to model E1 for the purpose of comparison, where $d_V=4\varepsilon/a_{sf}$.

three cases namely variable porosity, thermal dispersion and LTNE. A very large body of research works were analyzed and categorized for each of these areas.

The pertinent works within each area resulting in a true variance were selected within each category. The association between various models and the pertinent literature is given in Table 1. This comprehensive analysis resulted in Tables 2, 3, 4, and 5 for each of the presented categories. In the discussion of the results, the concentration is placed directly on the variances and mechanisms involved in creating these variances within each category. The physics of the two fundamental configurations considered here have been analyzed in detail in Vafai and Kim [3] and Amiri et al. [54] and will not be considered here.

4.1 Constant Porosity. Table 2 shows three variant models related to this category. Again, the corresponding references which form the variant models for this category as well as other categories are given in Table 1. The velocity and temperature profiles of the three different models are produced by solving the momentum and energy equations for the fundamental configuration shown in Fig. 1. As a result of using different variants of the Forchheimer and Brinkman terms in the momentum equation, the resultant velocity profiles for these models are expected to be different and consequently the heat transfer rate will also differ since the solution of the energy equation depends on the solution of the momentum equation.

A comprehensive study is performed to show the variations between the three different models by comparing the corresponding differences in velocity, temperature, and local Nusselt number distributions. The pertinent controlling parameters used for this category are porosity, inertia parameter, Darcy number, and Reynolds number. Figures 3–10 present a synthesis of variants for the models utilized within this category. The variations between the three variant models are found to be more visible in the velocity profiles which are shown in Figs. 3, 5, 7, and 9. The three models have an insignificant effect on the variations for the temperature and Nusselt number distributions as can be seen in Figs. 3–10. As such, the velocity profiles are used for comparing the three variant models within this category. The results reveal that the inertia parameter, porosity and the Darcy number have more a pro-

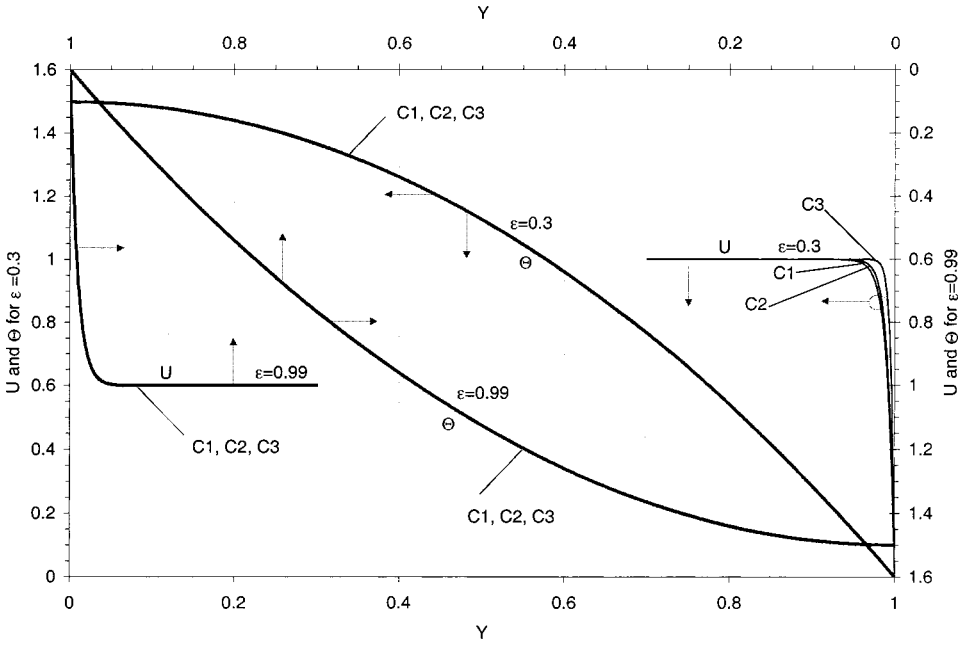

Fig. 3 Effect of porosity variations on velocity and temperature distributions for the constant porosity category [$\Lambda=10$, $\mathrm{Da}=10^{-4}$ and $\mathrm{Re}_H=100$]; (*a*) $\varepsilon=0.3$, (*b*) $\varepsilon=0.99$

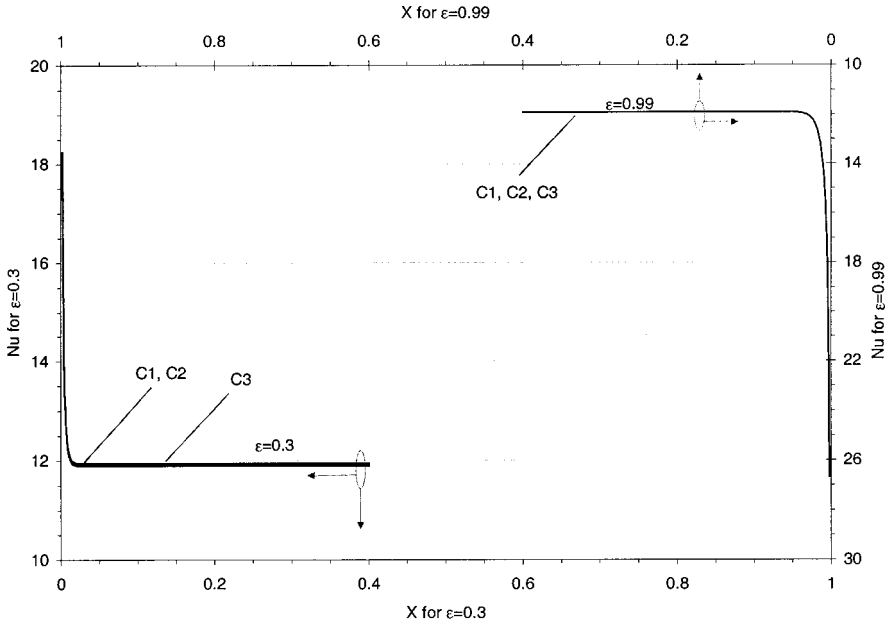

Fig. 4 Effect of porosity variations on Nusselt number distributions for the constant porosity category [$\Lambda=10$, $Da=10^{-4}$, and $Re_H=100$]; (*a*) $\varepsilon=0.3$, (*b*) $\varepsilon=0.99$

nounced effect on the convergence and the divergence of these models from each other even though the overall variations are relatively very small.

For the case of Darcy numbers corresponding to almost all practical applications, the three models are found to result in velocity and temperature fields which are quite close to each other for a given porosity or inertia parameter. Figure 5 shows that for a higher inertia parameter, the velocity profiles for the three models become closer to each other. It can be seen that models C1 and C2 become identical when the fluid inertia is negligible, i.e., $\Lambda=0$. This occurs because models C1 and C2 have the same Darcy and Brinkman terms which makes them the same when the

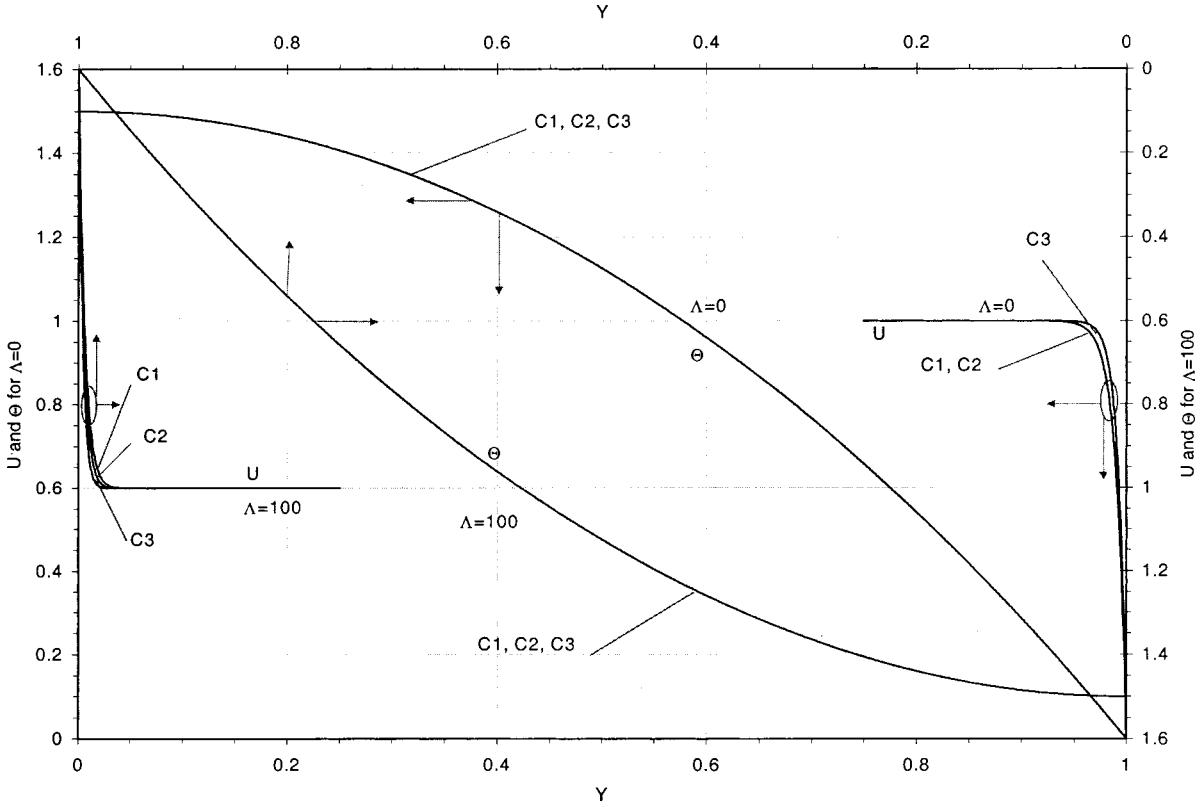

Fig. 5 Effect of the inertia parameter on velocity and temperature distributions for the constant porosity category [$\varepsilon=0.6$, $Da=10^{-4}$, and $Re_H=100$]; (*a*) $\Lambda=0$, (*b*) $\Lambda=100$

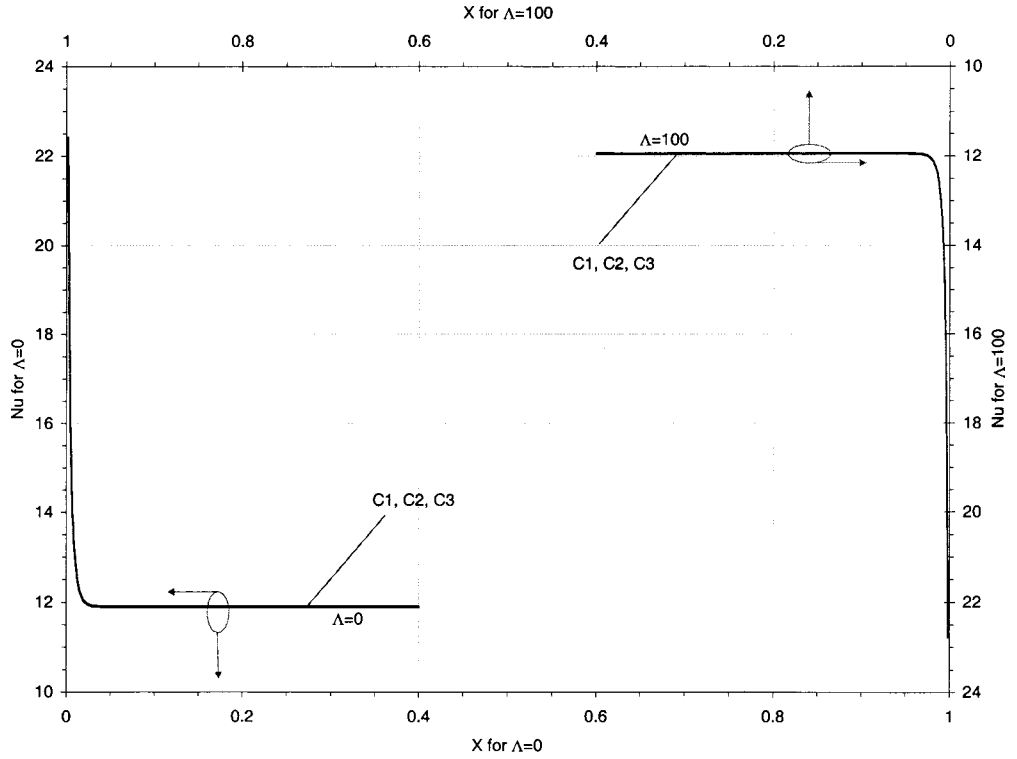

Fig. 6 Effect of the inertia parameter on Nusselt number distributions for the constant porosity category [ε=0.6, Da=10^{-4}, and Re_H=100]; (*a*) Λ=0, (*b*) Λ=100

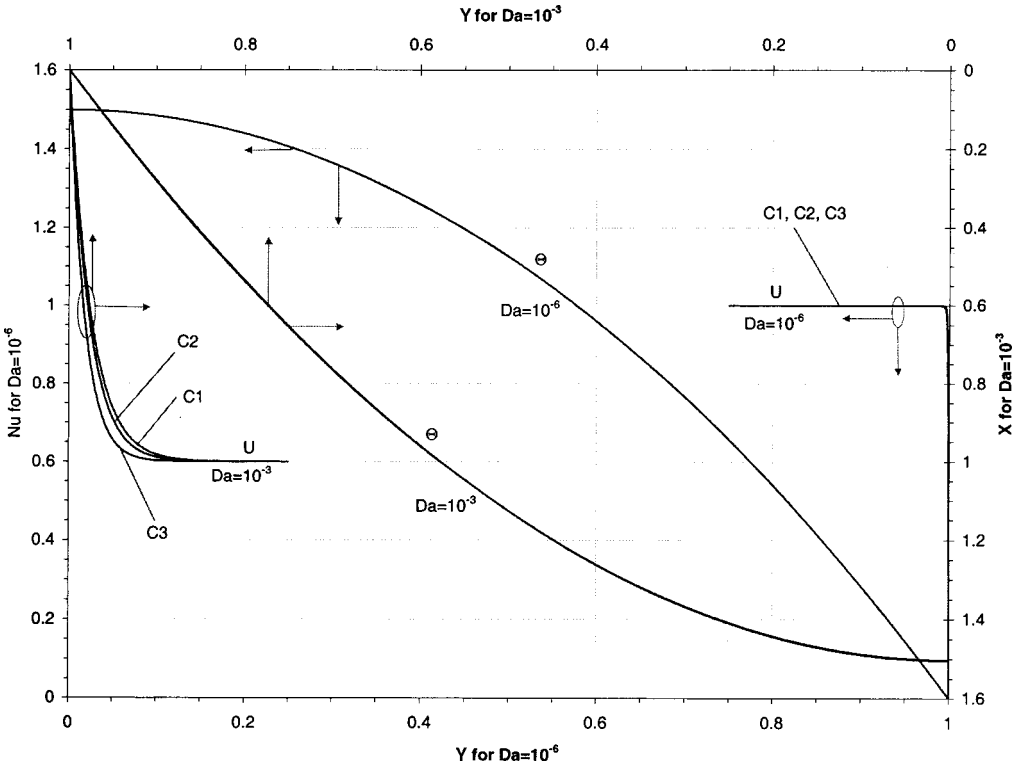

Fig. 7 Effect of Darcy number variations on velocity and temperature distributions for the constant porosity category [ε=0.6, Λ=10, and Re_H=100]; (*a*) Da=10^{-6}, (*b*) Da=10^{-3}

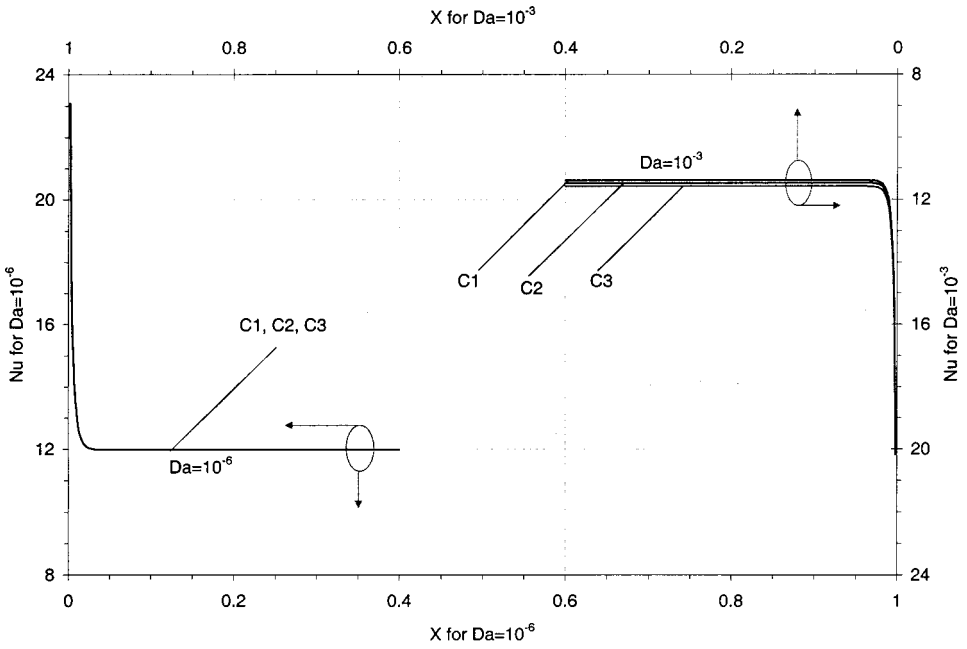

Fig. 8 Effect of Darcy number variations on Nusselt number distributions for the constant porosity category [ε=0.6, Λ=10, and Re_H=100]; (*a*) Da=10^{-6}, (*b*) Da=10^{-3}

Forchheimer term is ignored. It is relevant to mention that for high inertia parameter, the Forchheimer terms for models C2 and C3 are of the same order of magnitude as the Forchheimer term for model C1, while for low inertia parameters, the difference becomes more significant. It can be seen that for the case when the porosity of the porous medium approaches unity, the three models presented in Table 2 overlap and become identical as shown in Figs. 3–4. This happens because the presentations of the Darcy, Forchheimer, and Brinkman terms approach the same limit for all the three models when the porosity approaches unity.

It is clear that model C3 results in the thinnest momentum boundary layer while model C1 results in the thickest momentum

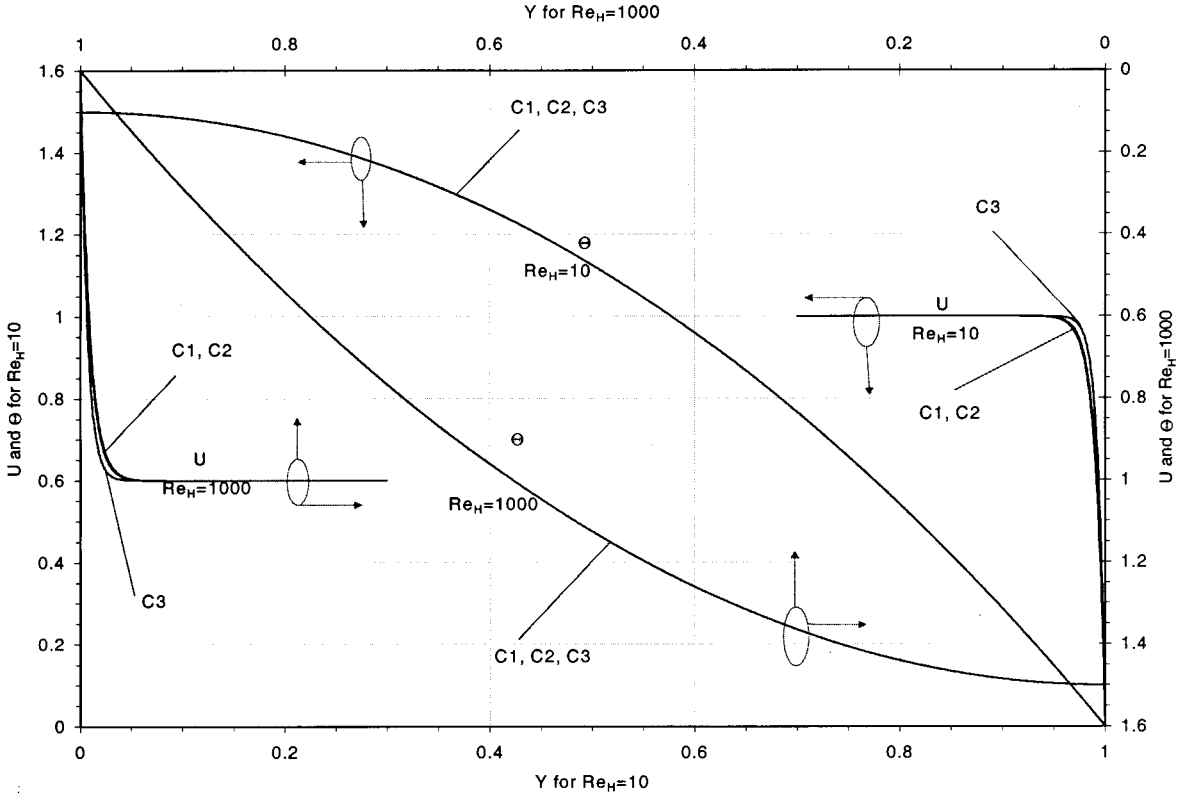

Fig. 9 Effect of Reynolds Number variations on velocity and temperature distributions for the constant porosity category [ε=0.6, Λ=10, and Da=10^{-4}]; (*a*) Re_H=10, (*b*) Re_H=1000

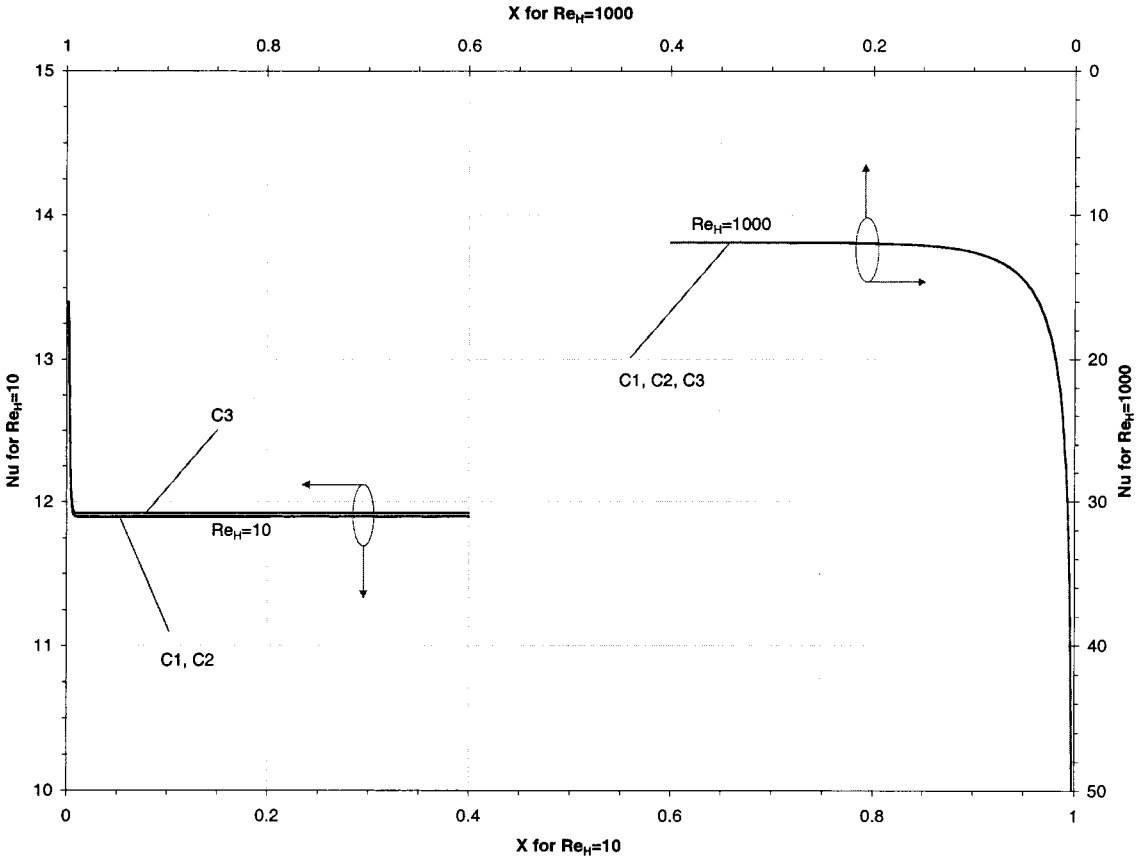

Fig. 10 Effect of Reynolds Number variations on Nusselt number distributions for the constant porosity category [ε=0.6, Λ=10, and Da=10^{-4}]; (*a*) Re$_H$=10, (*b*) Re$_H$=1000

boundary layer. This can be explained by first realizing that the Darcy terms are the same for the three variant models. Next, it should be noted that models C2 and C3 have similar Forchheimer terms; models C1 and C2 have similar Brinkman terms, while models C1 and C3 have different Forchheimer and Brinkman terms. Therefore, model C2 should fall in between the two other models as can be seen in Figs. 3–10. The reason that model C3 has the thinnest momentum boundary layer can be explained in terms of its Brinkman term formation which results in a smaller effective viscosity and a reduction in the shear stress between the fluid layers. On the other hand, model C1 has a smaller Forchheimer term which translates into less inertia than the other two models and as a result, the overall velocities of this model will be smaller. Therefore, the velocity profile for model C3 will appear as the upper bound; the velocity profile for model C1 will be the lower bound while model C2 will be in between for any condition.

Figures 3, 5, 7, and 9 show the velocity and temperature profiles for this category. It is clear that using different models has a substantially less impact on the temperature fields. Likewise, the Nusselt number profiles, as shown in Figs. 4, 6, 8, and 10 reveal that the three models result in very close agreements.

4.2 Variable Porosity. Four variant models have been found in literature for variable porosity media category as shown in Table 3. It can be seen that models V2 and V3 have the same Darcy and Forchheimer terms while the only difference between them is the presentation of the Brinkman terms. Models V1 and V4 have the same Forchheimer term, models V1 and V3 have the same Brinkman term while models V1, V2, and V3 have the same formation for the Darcy term. The pertinent parameters in this category are similar to those used by Vafai [30]. These parameters are the pressure gradient, the particle diameter, the freestream porosity, and the constants *b* and *c* in Eq. (4). Models V2 and V3 are closer to each other due to their similar representations for the Darcy and Forchheimer terms. On the other hand, models V1 and V4 are closer to each other due to similar Forchheimer terms. Figures 11–16 describe a synthesis of variants for the models utilized within the variable porosity category. Velocity profiles, temperature profiles, and Nusselt number profiles for this category are all shown in Figs. 11–16.

It has been shown in the literature (Vafai [30]) that an increase in the pressure gradient increases the centerline velocity and decreases the dimensionless velocity which is the ratio of the actual velocity to the centerline velocity. Also, an increase in the pressure gradient has been shown to form a thinner thermal boundary layer which leads to a higher Nusselt number. Figure 11 shows the effect of the pressure gradient on these four models for the variable porosity category. It can be seen that increasing the pressure gradient results in a closer agreement between models V1 and V4. Increasing the particle diameter causes the channeling effect to be more pronounced due to a reduction in fluid flow resistance near the solid boundary. These higher velocities increase the convected energy and form a thinner thermal boundary layer which leads to higher values of Nusselt number (Vafai [30]). The effect of the particle diameter on the nature of the four models can be seen in Fig. 12. It can be seen that an increase in the particle diameter causes a better agreement between models V1 and V4. The temperature profiles given in Fig. 12 show that an increase in the particle diameter results in closer agreement between all four models for the variable porosity category. This is due to the development of a thinner boundary layer which, in effect, masks out the variants within these four models.

Increasing the porosity causes the Darcy and Forchheimer terms within these models to approach the same limiting forms. Figure 13 shows that an increase in the freestream porosity results

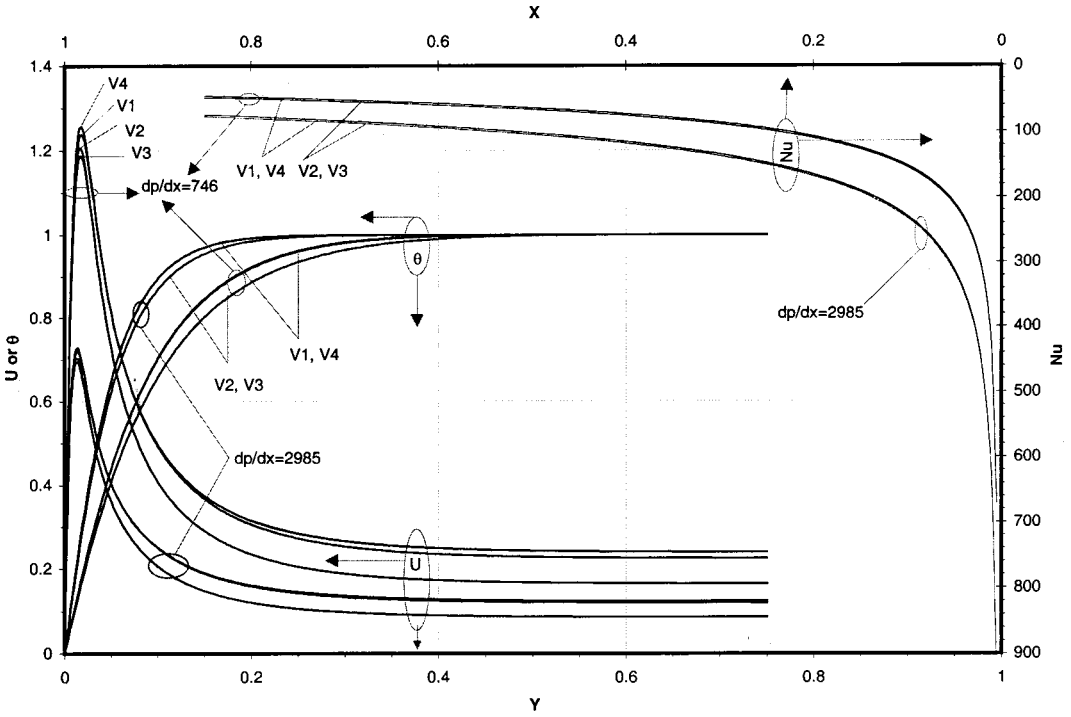

Fig. 11 Effect of pressure gradient on velocity, temperature and Nusselt number distributions for the variable porosity category [d_p=0.008, b=0.98, c=2.0, ε_∞=0.5]; (*a*) dp/dx=746, (*b*) dp/dx=2985

in a better agreement between these four models. That is, the overall difference between these four models diminishes as the freestream porosity increases. The effects of the constants b and c were discussed in Vafai [30]. It was found that an increase in b boosts the porosity near the walls while an increase in c causes more rapid decaying in the porosity resulting in a faster approach towards the freestream porosity value. Since increasing b and decreasing c increases the overall porosity, this effect is similar to increasing the freestream porosity. Therefore, increasing b and decreasing c creates a better agreement between these models. Figure 14 shows the effect of the constant c while Fig. 15 shows the effect of the constant b on the velocity profiles. A worse-case scenario for the divergence between these models is presented in Fig. 16 by combining the effects of a lower pressure gradient, lower freestream porosity, and smaller b and larger c, all of which enlarge the divergence between these four models. In contrast, the

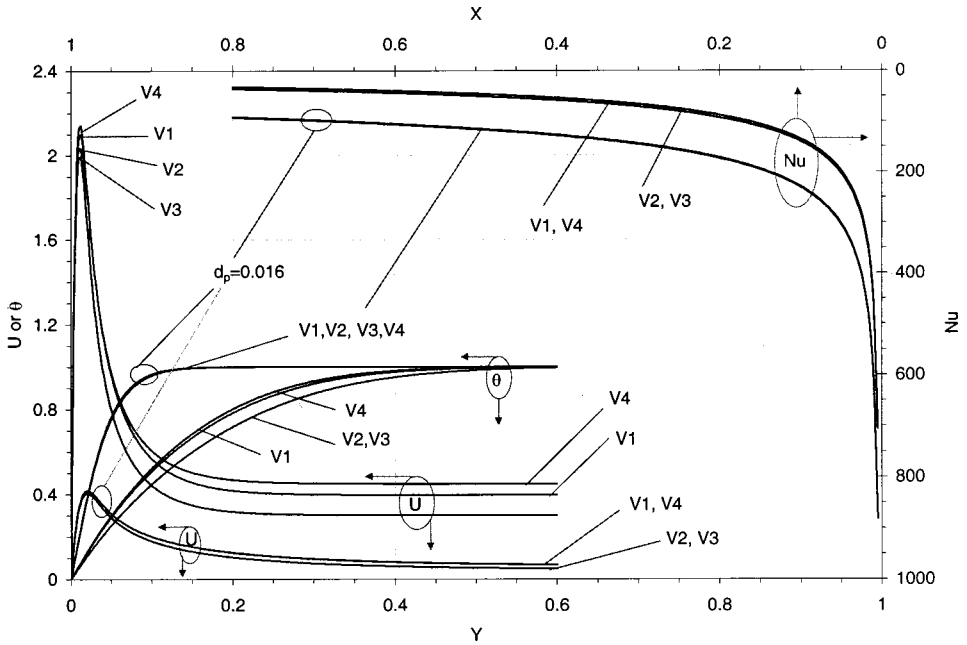

Fig. 12 Effect of particle diameter on velocity, temperature, and Nusselt number distributions for the variable porosity category [dp/dx=1493, b=0.98, c=2.0, ε_∞=0.5]; (*a*) d_p=0.004, (*b*) d_p=0.016

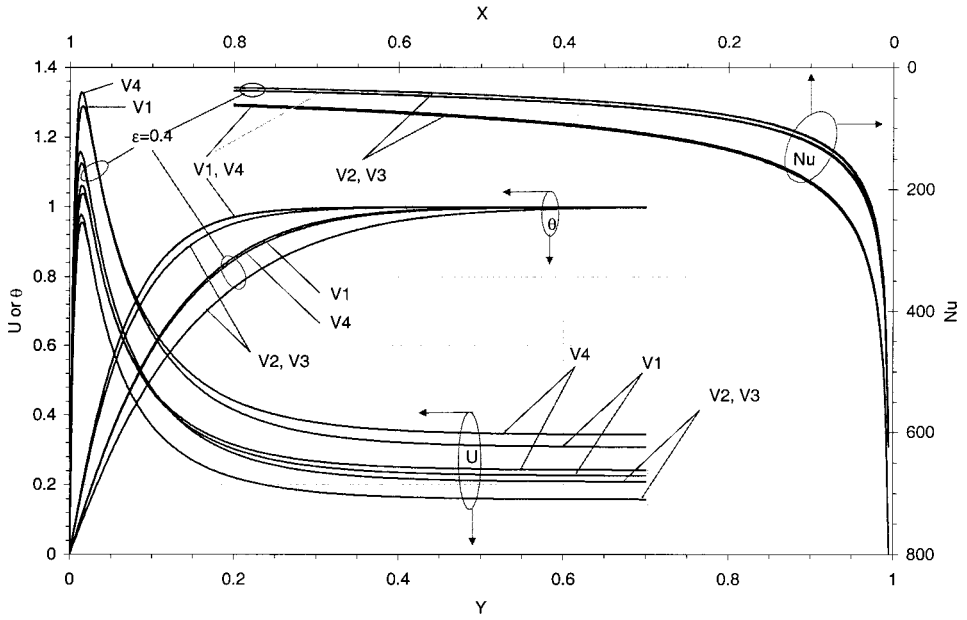

Fig. 13 Effect of freestream porosity on velocity, temperature, and Nusselt number distributions for the variable porosity category [$dp/dx=1493$, $d_p=0.008$, $b=0.98$, $c=2.0$]; (*a*) $\varepsilon_\infty=0.4$, (*b*) $\varepsilon_\infty=0.45$

effects of a higher pressure gradient, larger particle diameter, higher freestream porosity, larger b and smaller c, create a closer agreement between these four models, as seen in Fig. 16.

In general, models V2 and V3 result in velocity distributions which are quite close to each other except at the peak where V2 has a higher peak than model V3. This happens because model V2 has a lower effective viscosity than model V3 which translates to a lower resistance to fluid flow and consequently a higher peak. In general, models V1 and V4 are more similar and result in a larger freestream velocity when compared to models V2 and V3. This occurs because the Forchheimer term for the V2 and V3 models are larger than the corresponding one in the V1 and V4 models.

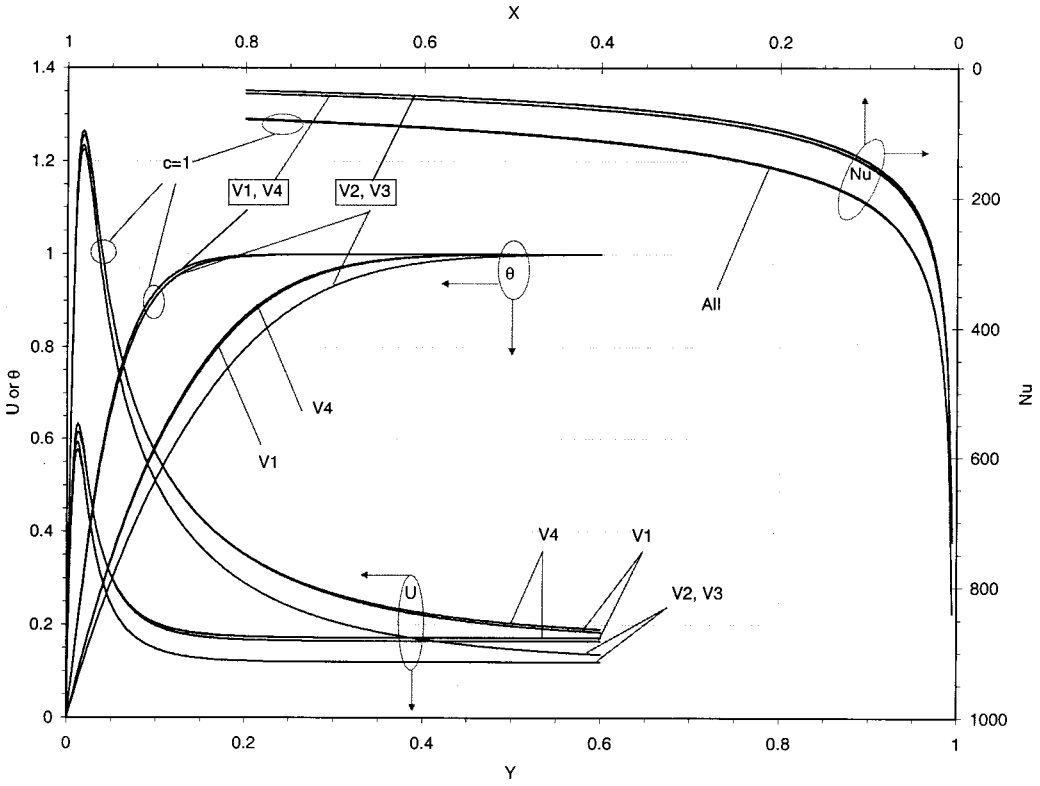

Fig. 14 Effect of constant c on velocity, temperature, and Nusselt number distributions for the variable porosity category [$dp/dx=1493$, $d_p=0.008$, $b=0.98$, $\varepsilon_\infty=0.5$]; (*a*) $c=1.0$, (*b*) $c=5.0$

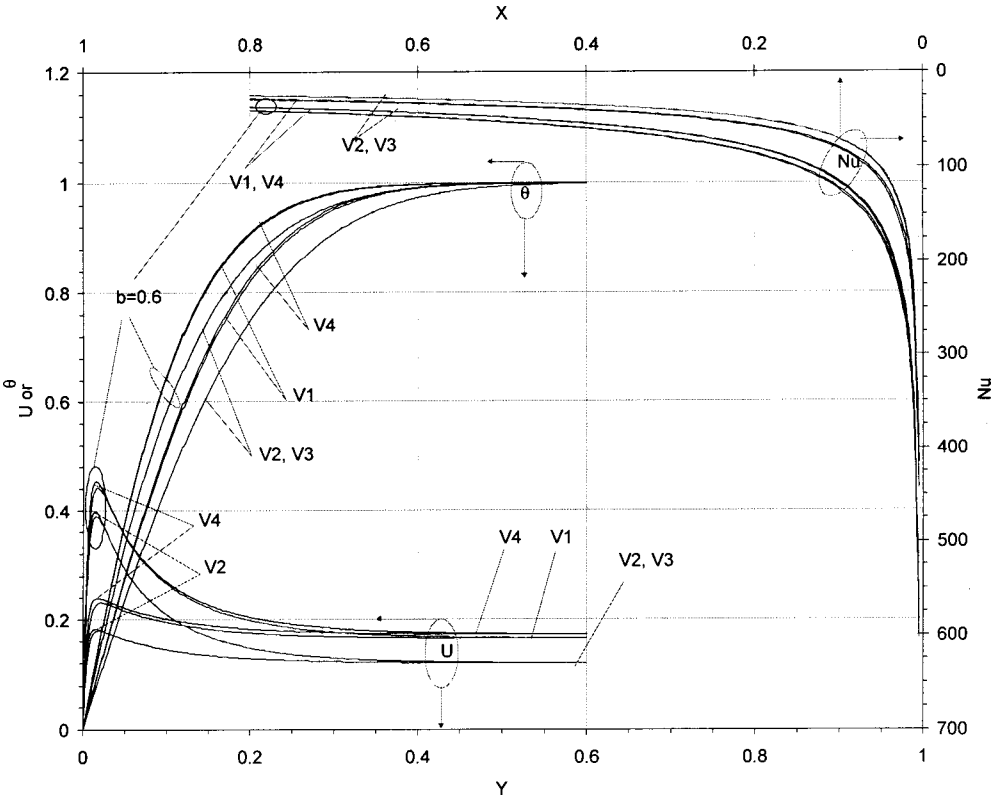

Fig. 15 Effect of constant *b* on velocity, temperature, and Nusselt number distributions for the variable porosity category [$dp/dx=1493$, $d_p=0.008$, $c=2.0$, $\varepsilon_\infty=0.5$]; (*a*) $b=0.2$, (*b*) $b=0.6$

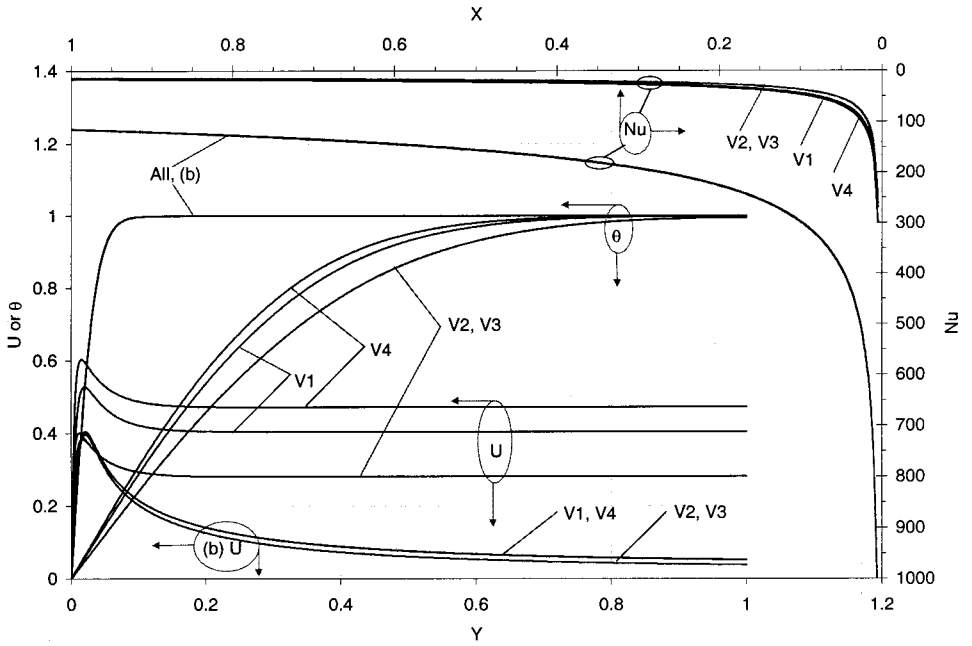

Fig. 16 Velocity, temperature, and Nusselt number distributions for the variable porosity category (*a*) $dp/dx=746$, $d_p=0.008$, $b=0.2$, $c=5.0$, $\varepsilon_\infty=0.4$; (*b*) $dp/dx=2985$, $d_p=0.016$, $b=0.98$, $c=1.0$, $\varepsilon_\infty=0.5$

4.3 Thermal Dispersion. The effect of thermal dispersion has been studied by a number of researchers in the past few years and has been shown to enhance the heat transfer process. These studies have tried to correlate the experimental data to a formulation for the thermal dispersion conductivity or diffusivity. A detailed analysis of the research works in this area reveals the existence of five pertinent models as displayed in Table 4. The present section considers the effects of using these five variant models for the transverse thermal dispersion conductivity on the transport processes in porous media. For this category, a constant porosity assumption was invoked since the variable porosity category was analyzed earlier.

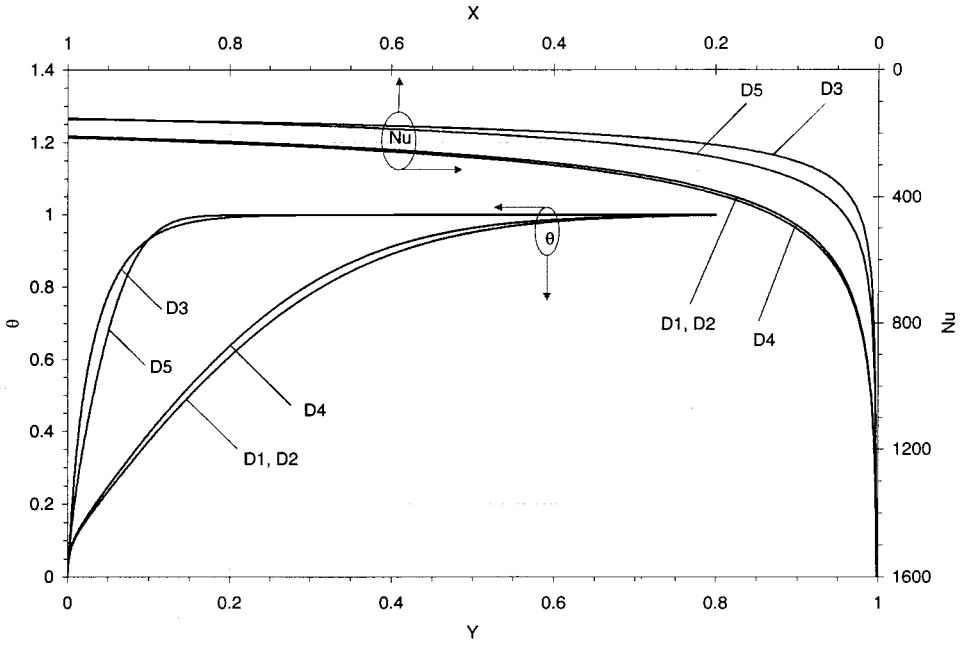

Fig. 17 Effect of porosity variations on temperature and Nusselt number distributions for the thermal dispersion category [ε=1/3.5, Λ=10, Da=10^{-4}, Re_p=100, and d_p=0.008]

Figures 17–24 present the effect of variations within the models utilized for the thermal dispersion category. Models D1 and D2 will be identical when the porosity equals 1/3.5 while models D1 and D4 will be identical when the porosity equals 0.27. Moreover, models D2 and D4 will be the same if the porosity of the porous medium is 0.25 as indicated in Fig. 19. In the present investigation, γ=0.1 was used for model D1, γ=0.04 was used for model D2, and γ=0.17 and w=1.5 were used for model D3. It is easier to observe the differences between models D1, D2, and D4. However, models D3 and D5 have different structures requiring a more careful set of comparisons. A comprehensive numerical study was performed to analyze the variances between the five cited models.

The effects of porosity, inertia parameter, Darcy number, Reynolds number, and the particle diameter on the variances within the thermal dispersion category are best illustrated in terms of their effects on the temperature and the local Nusselt number profiles. Changing the porosity has a significant effect on models D1, D2, and D4, while changing the Darcy number has a greater impact on model D5 since the permeability is directly a function of

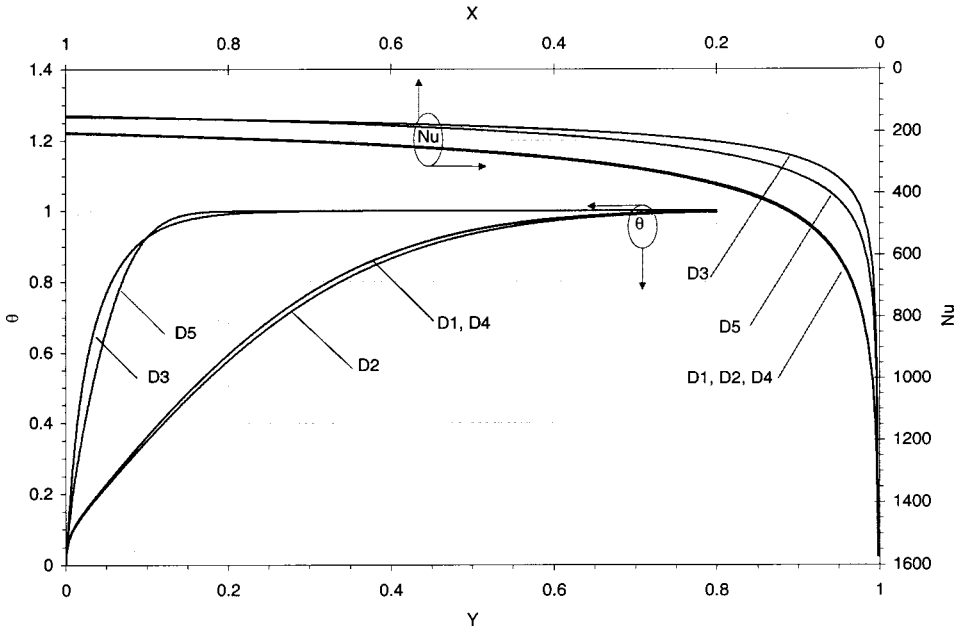

Fig. 18 Effect of porosity variations on temperature and Nusselt number distributions for the thermal dispersion category [ε=0.27, Λ=10, Da=10^{-4}, Re_p=100, and d_p=0.008]

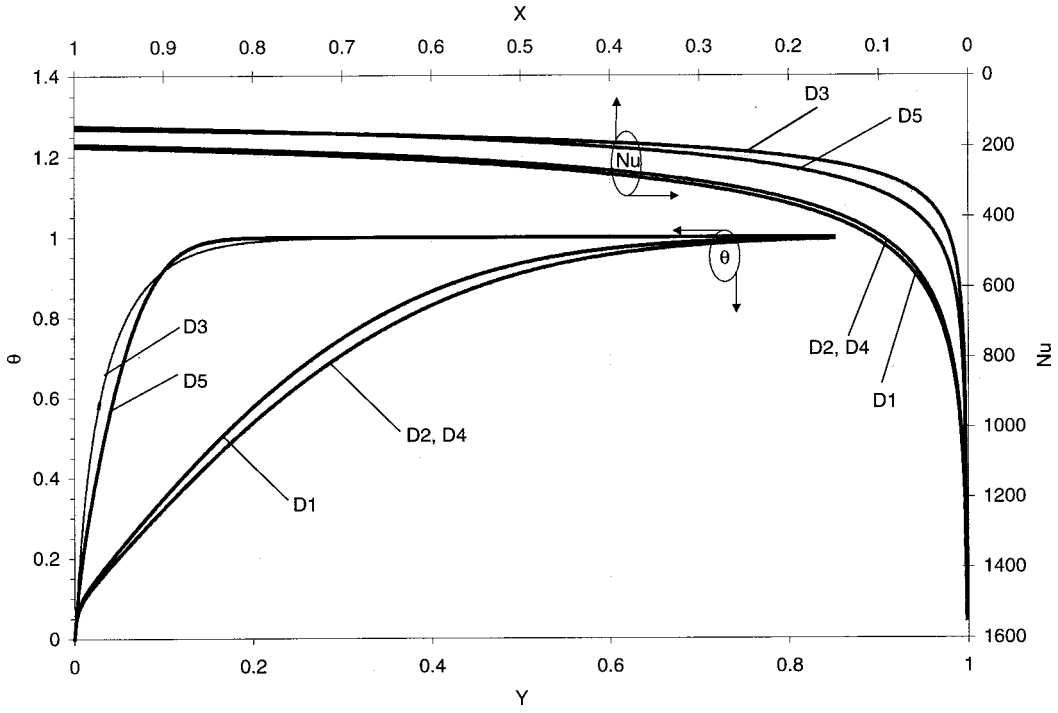

Fig. 19 Effect of porosity variations on temperature and Nusselt number distributions for the thermal dispersion category [ε=0.25, Λ=10, Da=10^{-4}, Re_p=100, and d_p=0.008]

the Darcy number. In general, model D3 has the thinnest thermal boundary layer while model D1 has the thickest boundary layer. Figures 17–20 show the effect of porosity on the temperature profiles and the Nusselt number profiles for the five dispersion models. It can be seen that models D1, D2, and D4 are affected by changing the porosity while the effect of porosity on models D3 and D5 is insignificant. The effect of the inertia parameter Λ is shown in Fig. 21, it can be seen that an increase in the inertia parameter causes a reduction in the disparity between the five models without changing the orders. This happens because the inertia parameter affects the velocity distribution and consequently affects the temperature and Nusselt number profiles. Since a velocity term appears in the expressions for the dispersion conductivity in all the five models, a change in the inertia parameter has an effect of the same order on the thermal dispersion for all of the five variant models.

As mentioned above, the Darcy number has a significant effect on model D5. This effect is shown in Fig. 22. Also, it can be seen

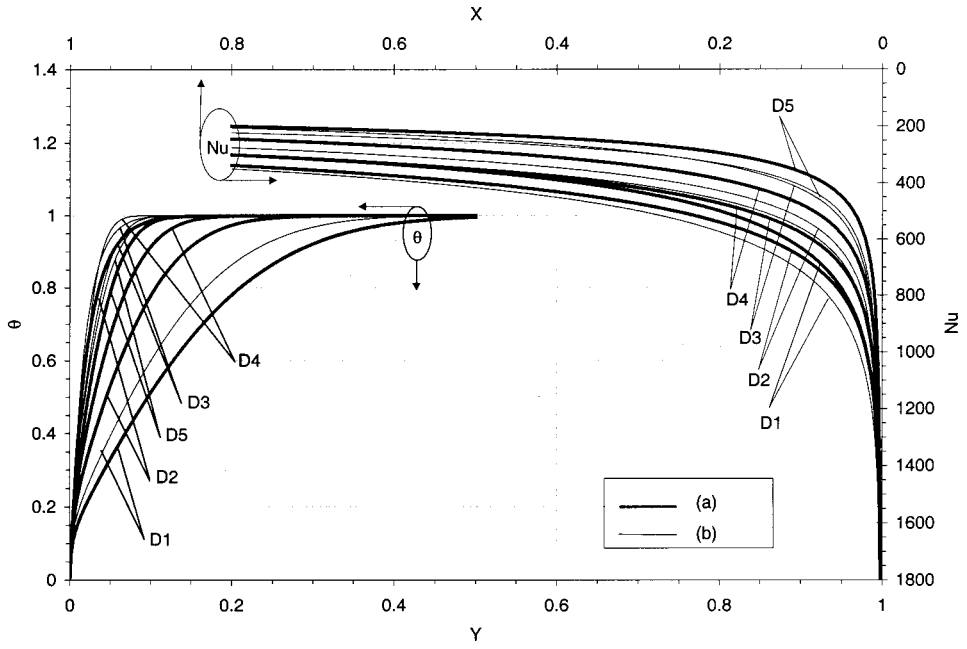

Fig. 20 Effect of porosity variations on temperature and Nusselt number distributions for the thermal dispersion category [Λ=10, Da=10^{-4}, Re_p=100, and d_p=0.008]; (*a*) ε=0.6, (*b*) ε=0.9

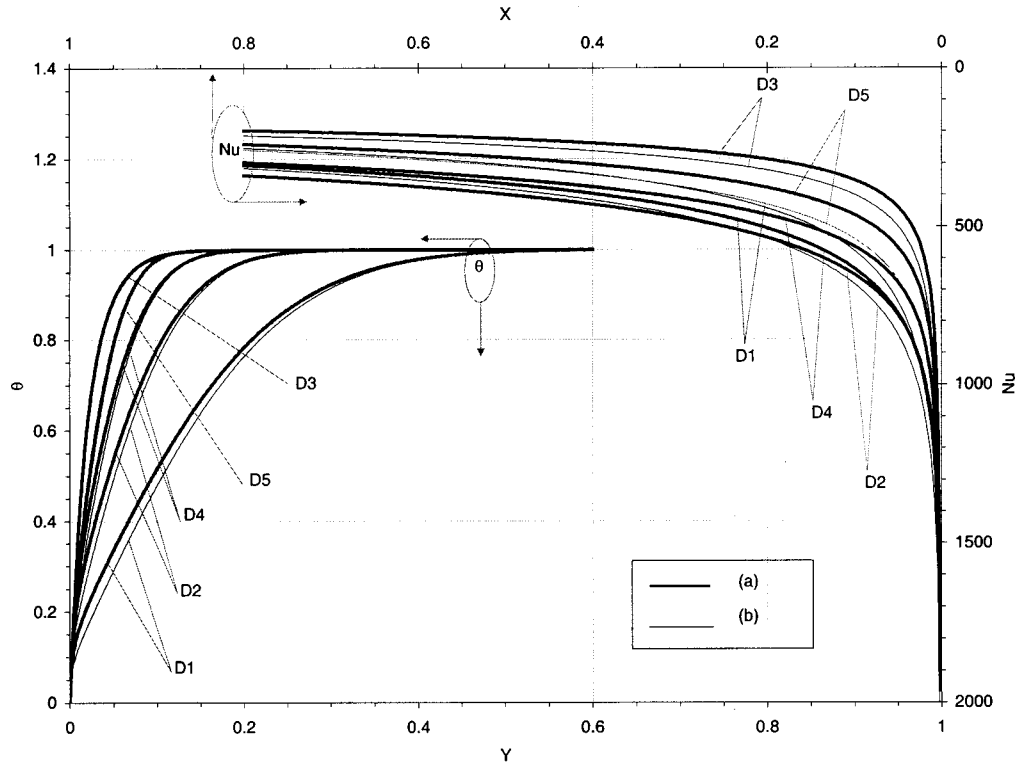

Fig. 21 Effect of inertia parameter variations on temperature and Nusselt number distributions for the thermal dispersion category [ε=0.6, Da=10^{-4}, Re_p=100, and d_p=0.008]; (*a*) Λ=0, (*b*) Λ=100

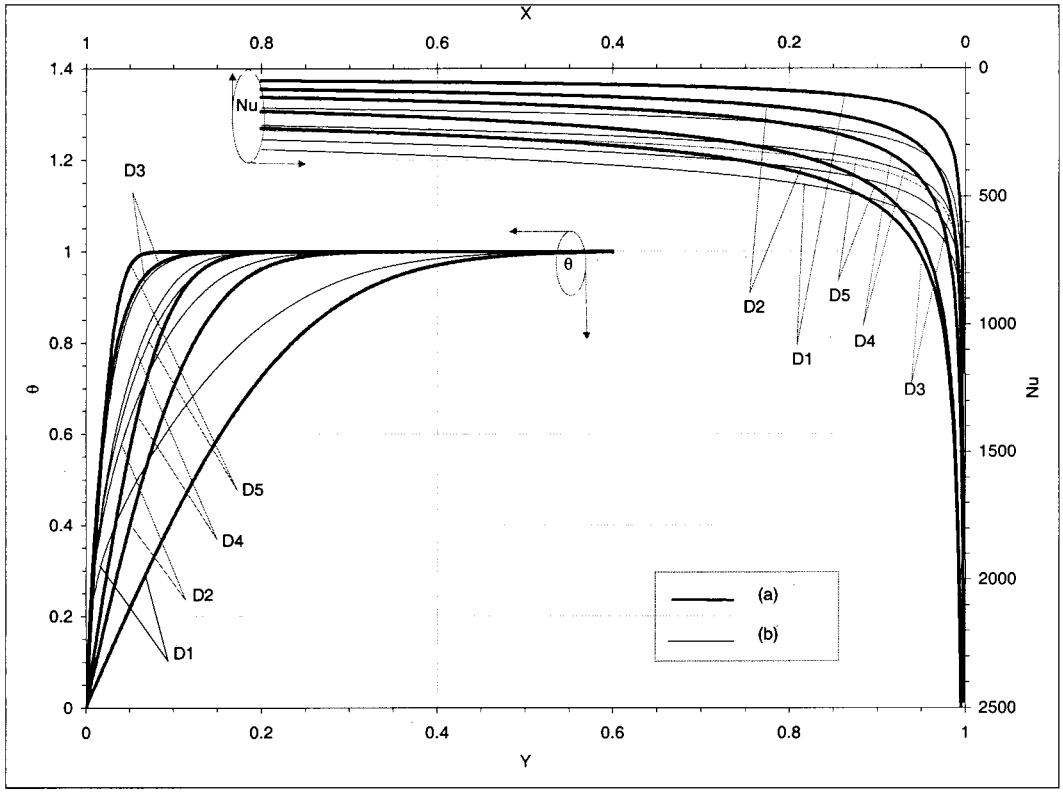

Fig. 22 Effect of Darcy number variations on temperature and Nusselt number distributions for the thermal dispersion category [ε=0.6, Λ=10, Re_p=100, and d_p=0.008]; (*a*) Da=10^{-7}, (*b*) Da=10^{-3}

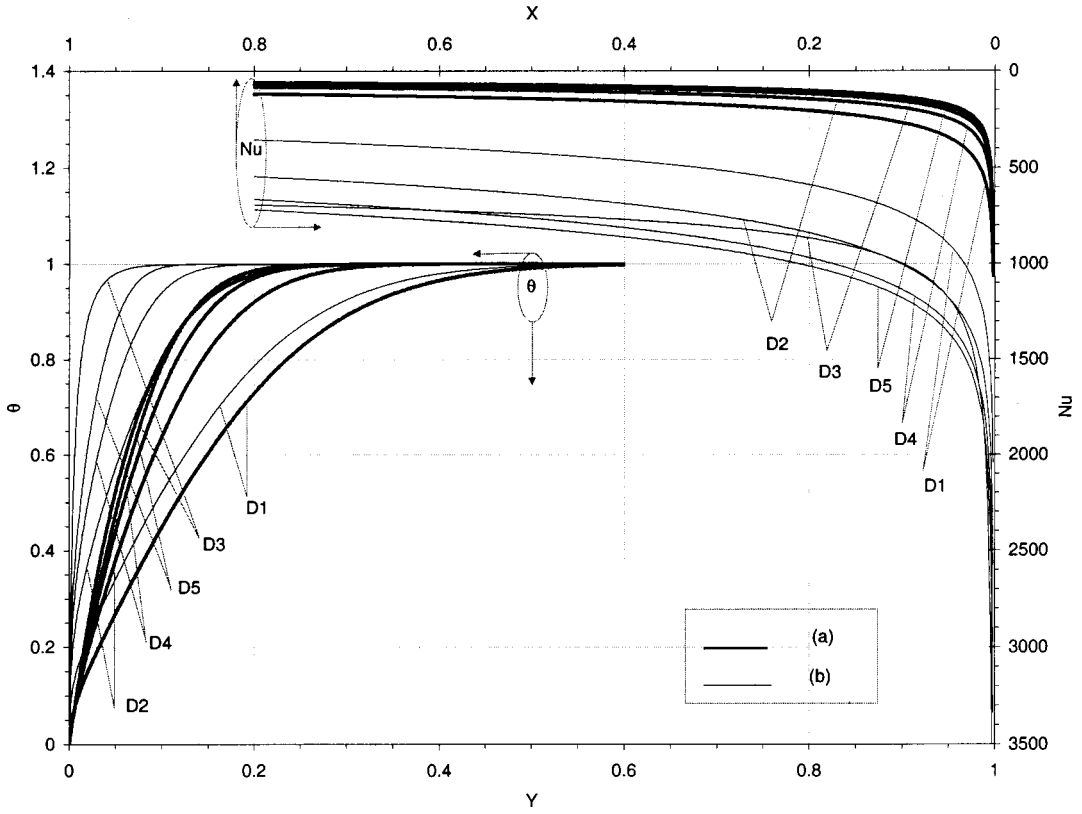

Fig. 23 Effect of Reynolds number variations on temperature and Nusselt number distributions for the thermal dispersion category [ε=0.6, Λ=10, Da=10^{-6}, and d_p=0.008]; (*a*) Re_p=10, (*b*) Re_p=1000

that an increase in the Darcy number, which is equivalent to an increase in the permeability, increases the thermal dispersion conductivity of model D5. The effect of increasing the Reynolds number on the thickness of the thermal boundary layers is shown in Fig. 23. Figure 23 shows the effect of Reynolds number on the Nusselt number distribution for the five dispersion models. It can be seen that at low Reynolds numbers model D3 establishes the lower bound for the heat transfer rate, while models D1 and D2 establish the upper bound. However, at high Reynolds numbers, models D1 and D2 establish the lower bound for the heat transfer rates. Finally, the effect of the particle diameter is found to be significant only for the first four models. This is due to the appearance of the particle diameter in the expressions for the thermal dispersion conductivity for these models. It can be seen from

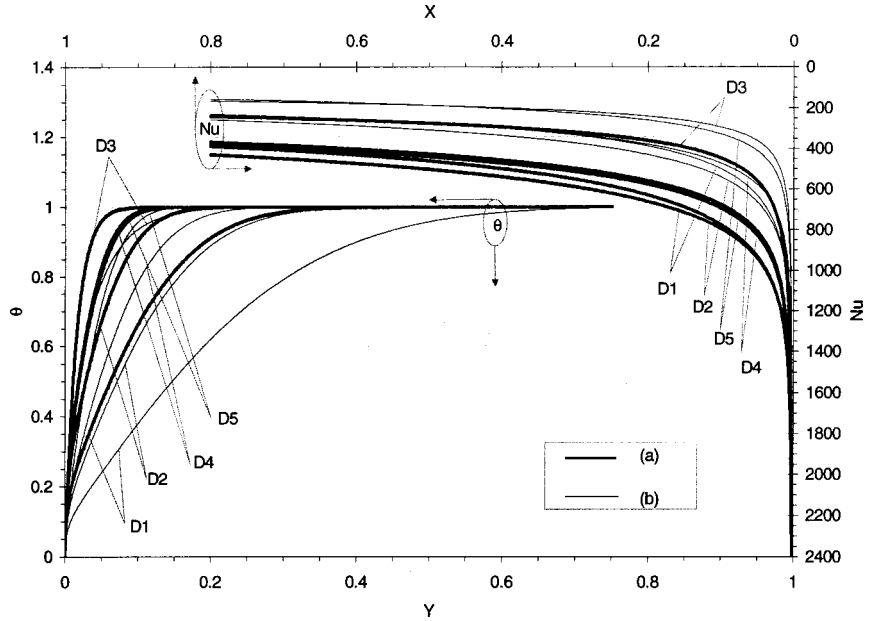

Fig. 24 Effect of particle diameter variations on temperature and Nusselt number distributions for the thermal dispersion category ε=0.6, Λ=10, Da=10^{-6}, and Re_p =100; (*a*) d_p=0.004, (*b*) d_p=0.016

Fig. 24 that model D5 is almost unaffected by changing the particle diameter while the other four models are significantly affected. Increasing the particle diameter enhances the thermal dispersion conductivity and consequently increases the heat transfer rate by causing a formation of a thinner thermal boundary layer.

4.4 Local Thermal Nonequilibrium. Table 5 shows three variant models for the fluid to solid heat transfer coefficient h_{sf} and for the specific surface area of the packed bed a_{sf}, corresponding to the pertinent investigations in the LTNE area. The effects of porosity, inertia parameter, Darcy number, Reynolds number, particle diameter, and ratio of fluid-to-solid conductivities on temperature and Nusselt number profiles for the models shown in Table 5 are analyzed.

Effects of porosity, inertia parameter, Darcy number, Reynolds number, particle diameter, and solid-to-fluid thermal conductivity changes on variances among these models are shown in Figs. 25–31. Porosity is expected to have an effect on the temperature distribution since a porosity term appears in a_{sf} for all the three models. Figure 25 shows the effect of porosity on the temperature distributions as well as the Nusselt number distributions for this category. The higher the porosity the smaller the variances among the three models. At low porosities models E2 and E3 are closer to each other. It is clear from the temperature profiles that the effect of the inertia parameter has an insignificant effect on the order of the thermal boundary layer for these models. However, a lower inertia parameter results in a closer agreement among the three models. Figure 26 shows the effect of the inertia parameter on the Nusselt number profiles. It is also found that the Darcy number also has an insignificant effect on the results. However, higher Darcy numbers cause slightly closer agreement among the models as seen in Fig. 27.

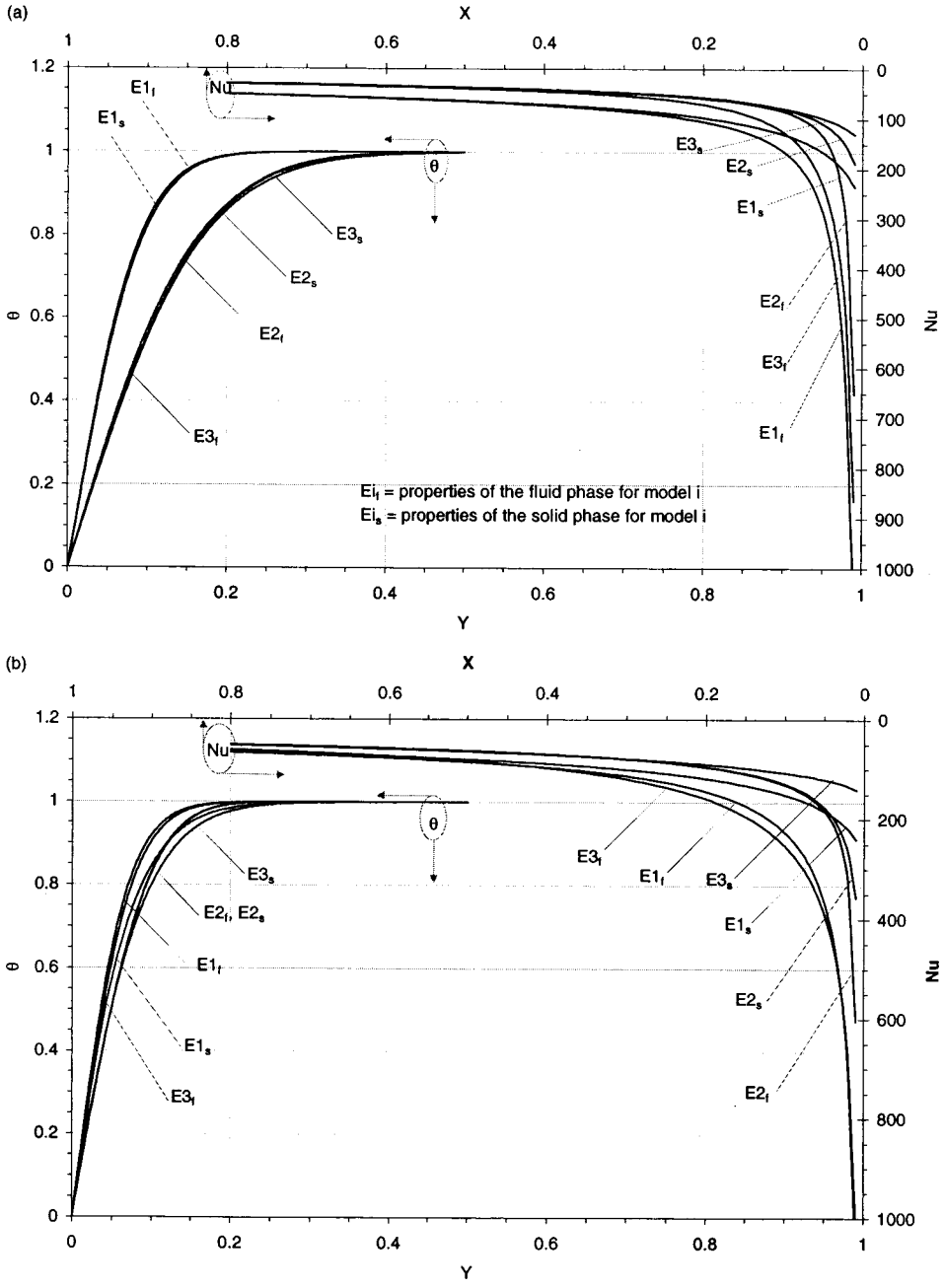

Fig. 25 Effect of porosity variations on temperature and Nusselt number distributions for the LTNE category [Λ=10, Da=10^{-4}, Re_P=100, d_P=0.008, k_s/k_f=25]; (*a*) ε=0.3, (*b*) ε=0.6

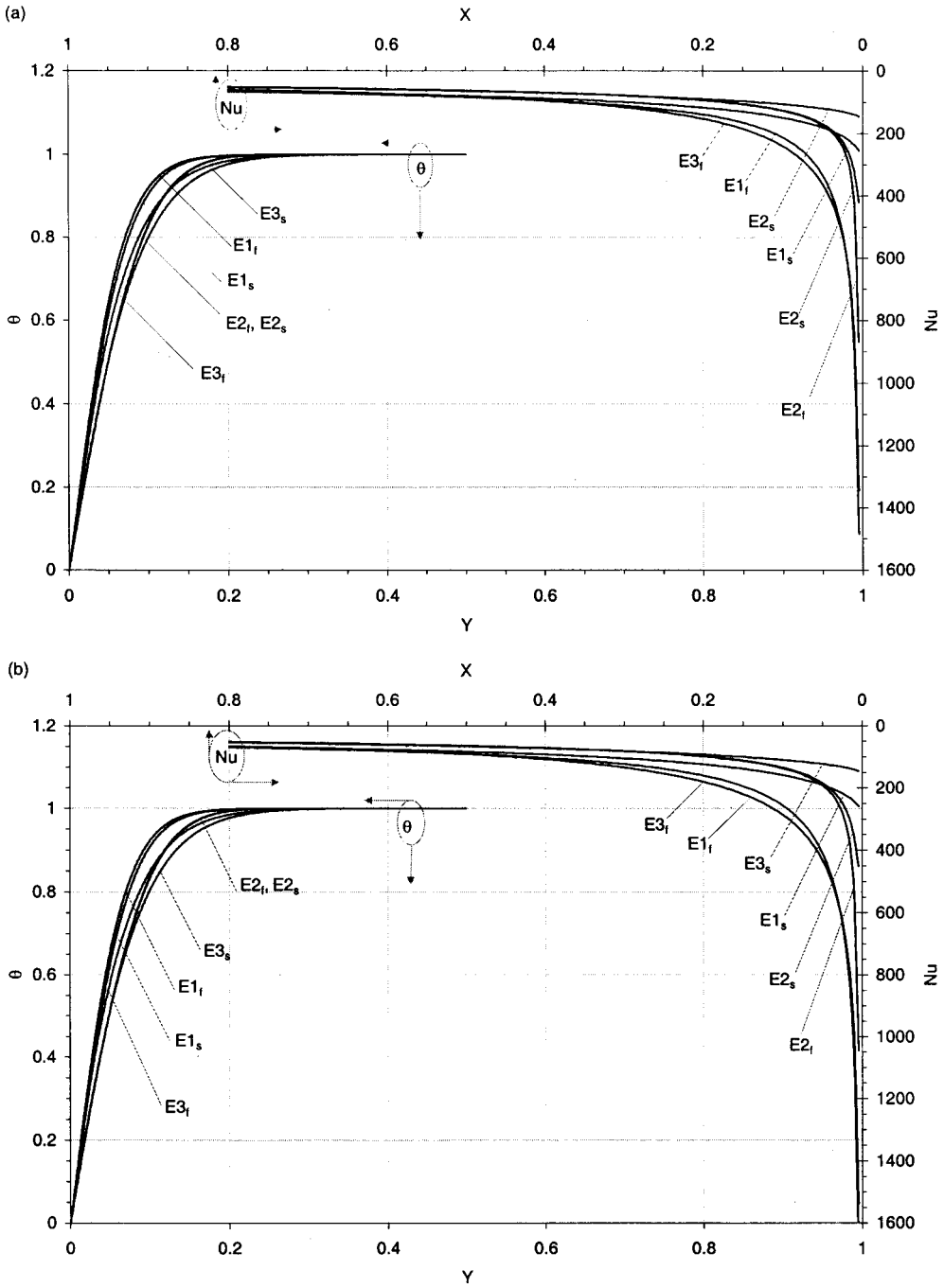

Fig. 26 Effect of inertia parameter variations on temperature and Nusselt number distributions for the LTNE category [ε=0.6, Da=10^{-4}, Re_P=100, d_P=0.008, k_s/k_f=25]; (*a*) Λ=0, (*b*) Λ=100

The Reynolds number is found to have a substantial effect on the variances among the three models. For higher Reynolds numbers the temperature profiles as well as Nusselt number distributions for the three models become closer to each other as shown in Fig. 28. The particle diameter appears in the expressions for h_{sf} and a_{sf} within all of the three models. Therefore, the effect of the particle diameter is expected to be critical. Smaller particle diameters encourage the LTE in models E1 and E3 while minimizing the variances among the three models. Larger particle diameters enhance the LTNE in models E1 and E3 while increasing the variances among the three models as seen in Fig. 29.

It should be noted that the thermal conductivities of the solid and fluid appear in the relationship for h_{sf} for model E3 while only the fluid phase conductivity appears in the h_{sf} equation for models E1 and E2. As such, the solid to fluid thermal conductivity ratio will have a significant effect on the variances among the three models. As seen in Fig. 30, a lower conductivity ratio enhances the LTE and reduces the variances among the three models. Figure 31 demonstrates two extreme conditions. In Fig. 31(*a*), all of the three models tend to be in local thermal equilibrium with very little variances among them, thus resulting in almost a single temperature profile. On the other hand, Fig. 31(*b*) shows conditions under which the LTNE as well as variances among the three models are substantially enhanced.

Recent investigations have made it possible to look at some additional physical effects regarding the thermal nonequilibrium. As such the works by Lee and Vafai [61] and Kuznetsov [62,58,63] can be cited. For example, in Kuznetsov [62–63] it

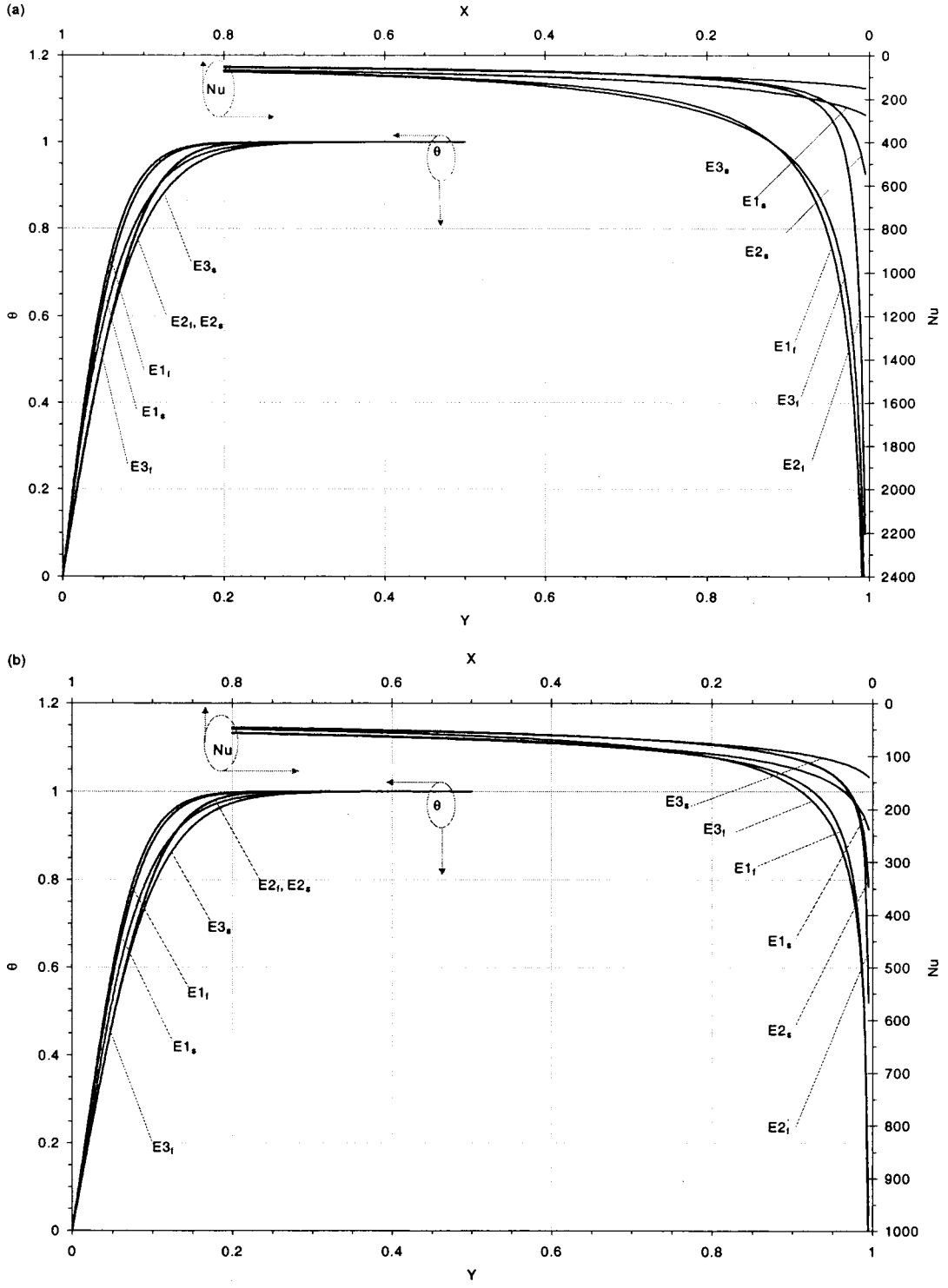

Fig. 27 Effect of Darcy number variations on temperature and Nusselt number distributions for the LTNE category [ε=0.6, Λ=10, Re_P=100, d_P=0.008, k_s/k_f=25]; (*a*) Da=10^{-8} (*b*) Da=10^{-3}

was shown that the temperature difference between the fluid and solid phases in forced convection flow through porous packed bed forms a wave whose amplitude is decreasing while propagating downstream.

A useful set of correlations for conversion of different models within each category is provided as follows.

$$\mathrm{Nu}_{C2}=0.9998\ \mathrm{Nu}_{C1}+0.23\varepsilon^{-1.173}\Lambda^{0.2812}\mathrm{Da}^{0.5357}\mathrm{Re}_H^{0.0636} \quad (11)$$

$$\mathrm{Nu}_{C3}=0.0002\ \mathrm{Nu}_{C1}+0.3664\varepsilon^{-1.2582}\mathrm{Da}^{0.45}\mathrm{Re}_H^{0.1788} \quad (12)$$

$$\mathrm{Nu}_{V2}=-3.927+1.2366\ \mathrm{Nu}_{V1}\left(\frac{dp}{dx}\right)^{-0.0041051} \times d_p^{0.0092769}(\varepsilon_\infty)^{0.1534}b^{0.0348}c^{-0.0218} \quad (13)$$

$$\mathrm{Nu}_{V3}=-4.6447+1.2441\ \mathrm{Nu}_{V1}\left(\frac{dp}{dx}\right)^{-0.005978} \times d_p^{0.0058872}(\varepsilon_\infty)^{0.1621}b^{0.0363}c^{-0.0228} \quad (14)$$

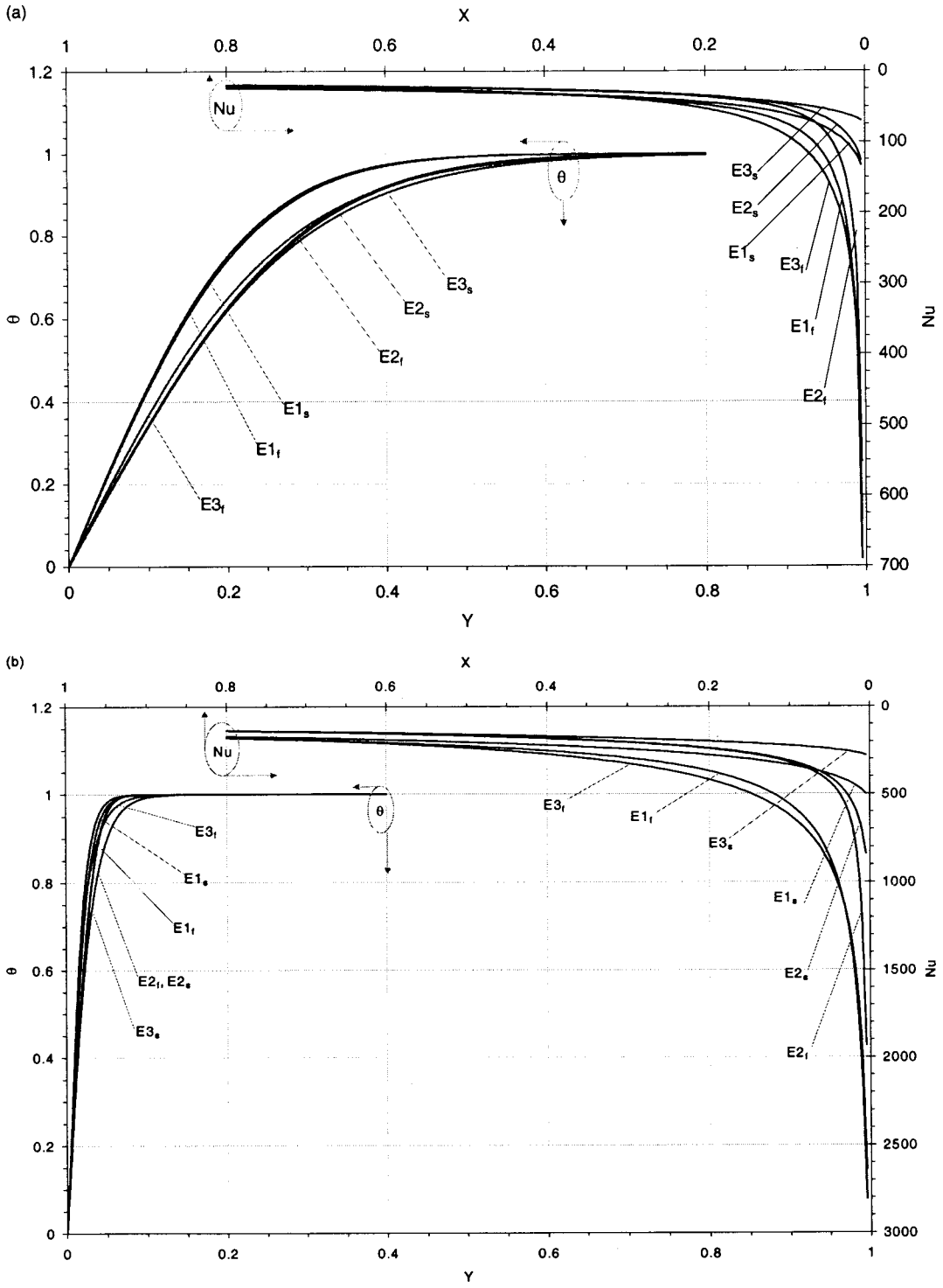

Fig. 28 Effect of Reynolds number variations on temperature and Nusselt number distributions for the LTNE category [ε=0.6, Λ=10, Da=10^{-4}, d_P=0.008, k_s/k_f=25]; (*a*) Re_P=10, (*b*) Re_P=1000

$$Nu_{V4} = 4.7358 + 0.9921\ Nu_{V1}\left(\frac{dp}{dx}\right)^{0.0125} \times d_p^{0.0152}(\varepsilon_\infty)^{0.0578} b^{0.0253} c^{-0.01} \quad (15)$$

$$Nu_{D2} = 4.8126 + 0.9898(4.8132 + Nu_{D1})^{0.9983} + 0.9581\varepsilon^{0.0634}\Lambda^{1.0442}Da^{0.7976}Re_p^{1.2389}d_p^{0.9967}Nu_{D1}^{1.0593} \quad (16)$$

$$Nu_{D3} = 29.5369 + 0.3445\varepsilon^{0.2447}(61.4249 + \Lambda)^{0.1497}Da^{-0.1152} \times Re_p^{0.511}d_p^{-0.2456}Nu_{D1}^{0.2314} \quad (17)$$

$$Nu_{D4} = 45.8467 + 0.8801\ Nu_{D1}^{0.9983} + 0.721\varepsilon^{-0.3152}\Lambda^{0.8653} \times Da^{0.7076}Re_p^{1.3521}d_p^{1.05}Nu_{D1}^{1.0548} \quad (18)$$

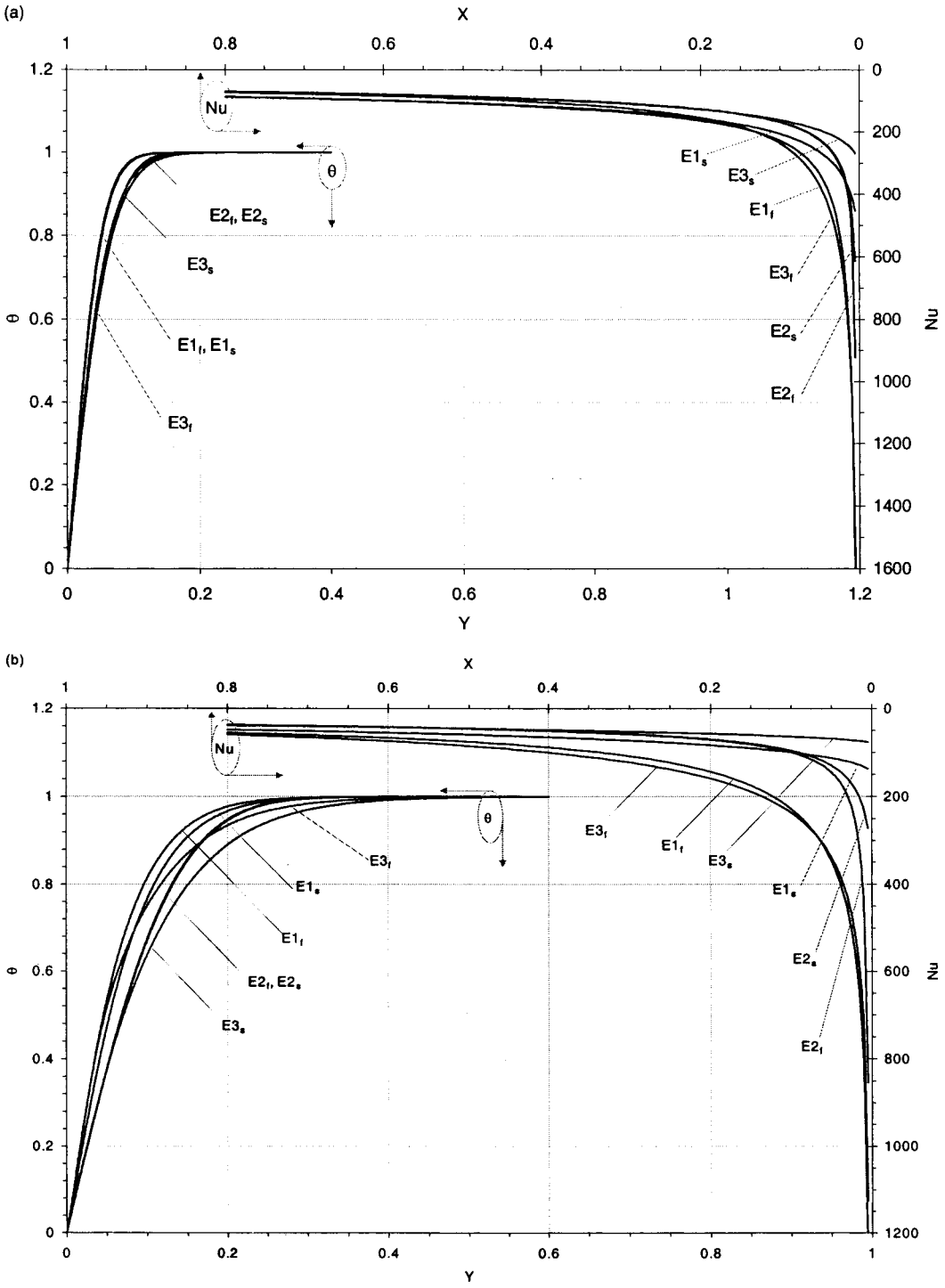

Fig. 29 Effect of particle diameter variations on temperature and Nusselt number distributions for the LTNE category [ε=0.6, Λ=10, Da=10^{-4}, Re_P=100, k_s/k_f=25]; (*a*) d_P=0.004, (*b*) d_P=0.016

$$Nu_{D5} = -71.2195 + 0.137\varepsilon^{0.2971}(389.0253+\Lambda)^{0.4933} \times Da^{-0.0354} Re_p^{0.3744} d_p^{-0.3873} Nu_{D1}^{0.2098} \quad (19)$$

$$Nu_{E2f} = 2.4262 + 1.2043(Nu_{E1f})^{0.8152} + 0.7792\varepsilon^{0.2.2892}\Lambda^{0.0485} \times Da^{0.1749} Re_p^{0.1567} d_p^{-0.0531} \left(\frac{k_s}{k_f}\right)^{-0.4402} (Nu_{E1f})^{1.268} \quad (20)$$

$$Nu_{E3f} = -77.5642 + 0.2554(Nu_{E1f})^{1.1645} + 81.2051\varepsilon^{0.5343}(0.3576+\Lambda)^{0.0139} Da^{-0.0201} \times Re_p^{0.1605} d_p^{0.0328} \left(\frac{k_s}{k_f}\right)^{-0.0019348} \quad (21)$$

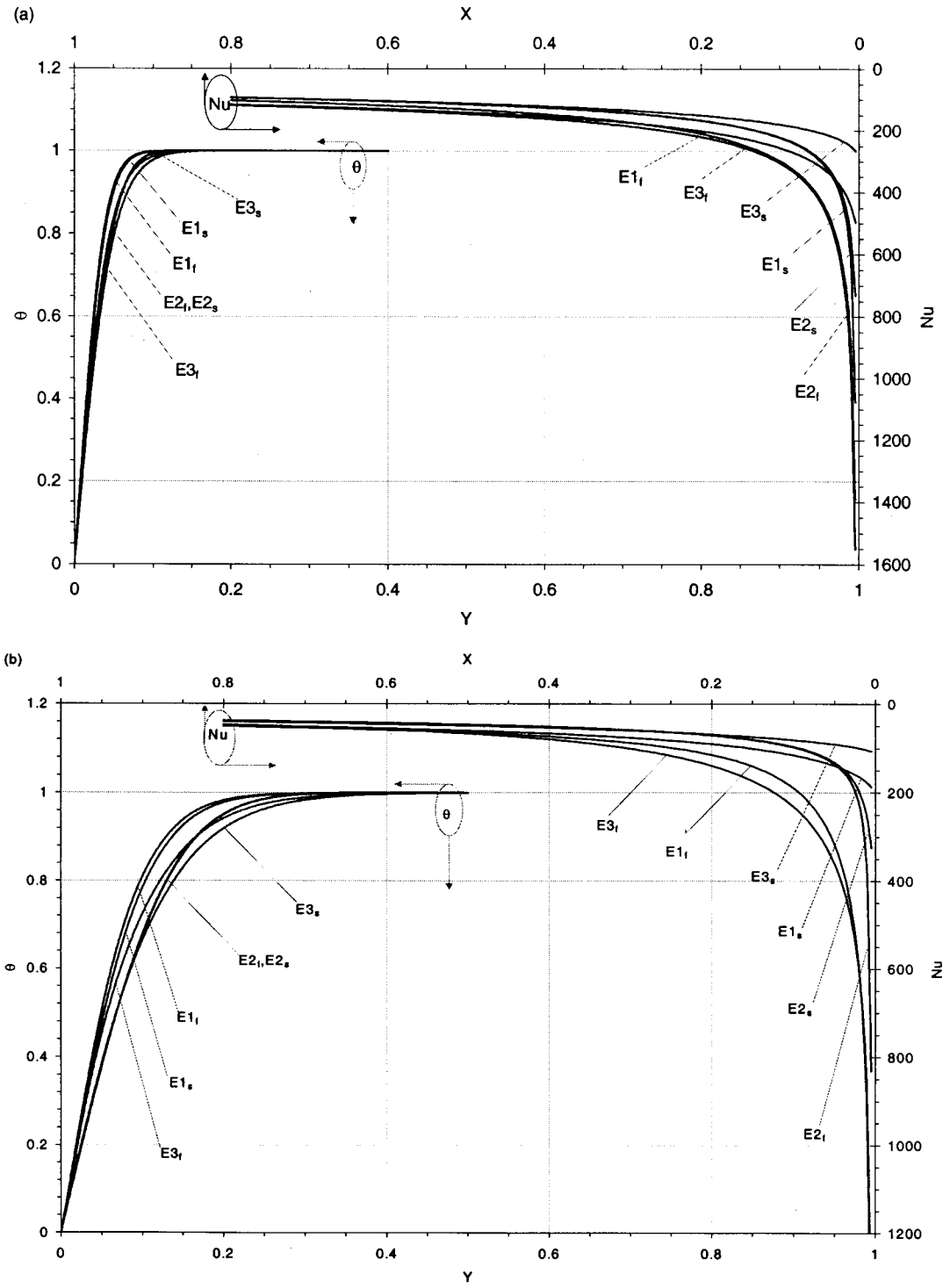

Fig. 30 Effect of solid-to-fluid thermal conductivity ratio variations on temperature and Nusselt number distributions for the LTNE category [ε=0.6, Λ=10, Da=10^{-4}, Re_P=100, d_P=0.008]; (*a*) k_s/k_f=5, (*b*) k_s/k_f=50

$$\mathrm{Nu}_{\mathrm{E2}s} = -10.5362 + 1.7505(\mathrm{Nu}_{\mathrm{E1}s})^{0.8054} + 0.0515\varepsilon^{1.469}\mathrm{Da}^{0.0187}\mathrm{Re}_p^{-0.3453} \times d_p^{0.6346}\left(\frac{k_s}{k_f}\right)^{0.3848}(\mathrm{Nu}_{\mathrm{E1}s})^{2.2807} \quad (22)$$

$$\mathrm{Nu}_{\mathrm{E2}s} = -9.566 + 0.7751(\mathrm{Nu}_{\mathrm{E1}s})^{0.9753} + 28.018\varepsilon^{1.6719} \times (0.0463+\Lambda)^{0.0154}\mathrm{Da}^{-0.011}\mathrm{Re}_p^{0.7615}d_p^{-1.1829}\left(\frac{k_s}{k_f}\right)^{-0.6435} \times (\mathrm{Nu}_{\mathrm{E1}s})^{-1.5} \quad (23)$$

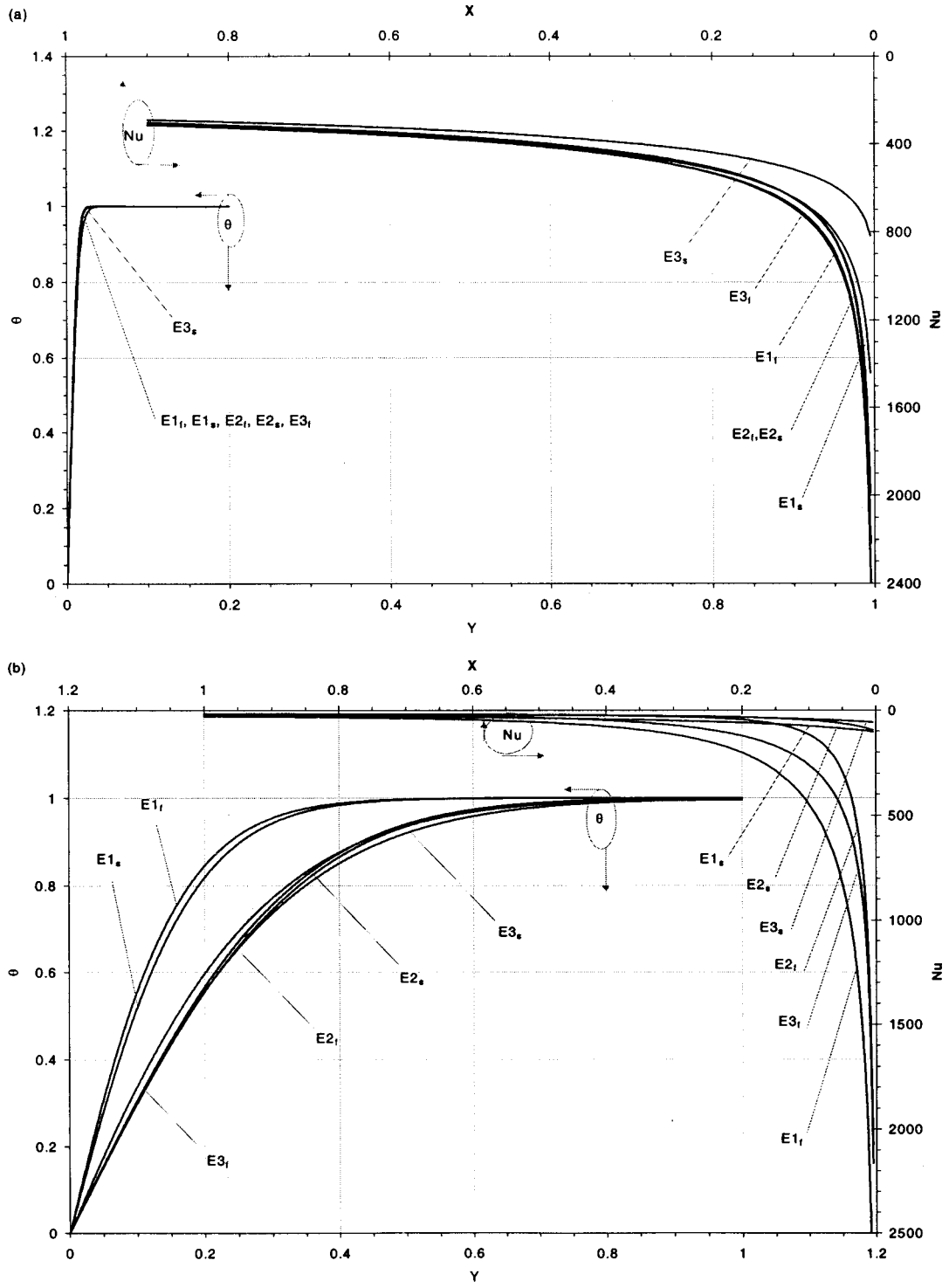

Fig. 31 Temperature and Nusselt number distributions for the LTNE category; (*a*) $\varepsilon=0.9$, $\Lambda=0$, Da $=10^{-3}$, $Re_P=1000$, $d_P=0.004$, $k_s/k_f=5$, (*b*) $\varepsilon=0.3$, $\Lambda=100$, $Da=10^{-8}$, $Re_P=100$, $d_P=0.016$, $k_s/k_f=50$

Equations (11) and (12) convert the results from models C2 and C3 to model C1 for the constant porosity category. Equations (13), (14) and (15) convert the results from models V2, V3, and V4 to model V1 for the variable porosity category. Equations (16), (17), (18), and (19) convert the results from models D2, D3, D4, and D5 to model D1 for the thermal dispersion category. Finally, Eqs. (20), (21), (22), and (23) convert the results from models E2 and E3 to model E1 for the local thermal nonequilibrium category.

5 Conclusions

A comprehensive comparative study of the models for transport processes through a porous medium was performed. Four major categories namely constant porosity, variable porosity, thermal dispersion, and local thermal nonequilibrium were analyzed in detail. The main objective of the present study was to analyze the variances among these models within each category. The results of this investigation systematically quantify and characterize the

effects of the pertinent controlling parameters on the variances among different models. It is shown that for some cases the variances within different models have a negligible effect on the results, while for some cases the variations can become significant. In general, the variances have a more pronounced effect on the velocity field and a substantially smaller effect on the temperature field and Nusselt number distribution.

The variants among models for the constant porosity and the variable porosity categories are generally small and are anticipated to be well within experimental uncertainties. As such, these models can be considered to have negligible variances amongst them. On the other hand, the variants among models for the thermal dispersion category are found to be more pronounced. For small porosities, models D1, D2, and D4 are close to each other while for large porosities, models D2, D3, D4, and D5 are close to each other. For small inertia parameters, model D1 and D4 are found to be close to each other while for large inertia parameters, models D1 and D5 are closer to each other. For low Reynolds numbers, models D3 and D5 are close to each other. For small particle diameters, models D1, D4, and D5 are found to be closer to each other. Finally, the variants among models for the local thermal nonequilibrium category are not substantial and are generally more pronounced within the entry region and well within experimental uncertainties. However, model E1 differs from models E2 and E3 for the cases of small porosities and low Reynolds numbers. It should be noted that a detailed analysis of different types of interfacial conditions between a porous medium and a fluid layer was also recently investigated by Alazmi and Vafai [64].

Nomenclature

a_{sf} = specific surface area of the packed bed, m^{-1}
b, c = porosity variation parameters, Eq. (4)
C_p = specific heat at constant pressure, J kg^{-1} K^{-1}
d_p = particle diameter, m
d_v = parameter defined in Table 5
Da = Darcy number, K/H^2
F = geometric function defined in Eq. (3)
h_{sf} = fluid-to-solid heat transfer coefficient, W m^{-2} K^{-1}
H = half the height of the packed bed, m
k = thermal conductivity, W m^{-1} K^{-1}
K = permeability, m^2
L = length of the packed bed, m
Nu = local Nusselt number, hD_h/k_{eff}
Nu = average Nusselt number
Pe = Peclet number, $u_c d_p/\alpha_f$
Pr = Prandtl number, $\mu C_{Pf}/k_f$
Re_H = Reynolds number, $u_c H/\nu$
Re_p = particle Reynolds number, $u_c d_p/\nu$
T = temperature, K
u = velocity in x-direction, m s^{-1}
U = nondimensional velocity, u/u_c
x, y = Cartesian coordinates, m
X, Y = nondimensional coordinates, x/H and y/H

Greek Symbols

α = thermal diffusivity, m^2 s^{-1}
γ = dispersion coefficient parameter
ε = porosity
Λ = inertia parameter, $\varepsilon^{3/2} F u_\infty H/\nu_f$
μ = kinematics viscosity, kg m^{-1} s^{-1}
ν = dynamic viscosity, m^2 s^{-1}
θ = dimensionless temperature, $(T_w - T)/(T_w - T_e)$
Θ = dimensionless temperature, $h(T_w - T)/q_w$

Subscripts

c = convective component
d = dispersion
e = inlet
eff = effective property
f = fluid
s = solid
w = wall
∞ = freestream

References

[1] Vafai, K., and Tien, C. L., 1981, ''Boundary and Inertia Effects on Flow and Heat Transfer in Porous Media,'' Int. J. Heat Mass Transf., **24**, pp. 195–203.
[2] Vafai, K., and Tien, C. L., 1982, ''Boundary and Inertia Effects on Convective Mass Transfer in Porous Media,'' Int. J. Heat Mass Transf., **25**, pp. 1183–1190.
[3] Vafai, K., and Kim, S. J., 1989, ''Forced Convection in a Channel Filled With a Porous Medium: An Exact Solution,'' ASME J. Heat Transfer, **111**, pp. 1103–1106.
[4] Hadim, A., 1994, ''Forced Convection in a Porous Channel With Localized Heat Sources,'' ASME J. Heat Transfer, **116**, pp. 465–472.
[5] Kaviany, M., 1985, ''Laminar flow through a porous channel bounded by isothermal parallel plates,'' Int. J. Heat Mass Transf., **28**, pp. 851–858.
[6] Lauriat, G., and Vafai, K., 1991, ''Forced Convective Flow and Heat Transfer Through a Porous Medium Exposed to a Flat Plate or a Channel,'' *Convective Heat and Mass Transfer in Porous Media*, S. Kacac, B. Kilikis, F. A. Kulacki, and F. Arnic, eds., Kluwer Academic, Dordrecht, pp. 289–328.
[7] Beckermann, C., and Viskanta, R., 1987, ''Forced Convection Boundary Layer Flow and Heat Transfer Along a Flat Plate Embedded in a Porous Medium,'' Int. J. Heat Mass Transf., **30**, pp. 1547–1551.
[8] Kim, S. J., and Choi, C. Y., 1996, ''Convective Heat Transfer in Porous and Overlying Fluid Layers Heated From Below,'' Int. J. Heat Mass Transf., **39**, pp. 319–329.
[9] Kladias, N., and Prasad, V., 1990, ''Flow Transitions in Buoyancy-Induced Non-Darcy Convection in a Porous Medium Heated From Below,'' ASME J. Heat Transfer, **112**, pp. 675–684.
[10] Nield, D. A., Junqueira, S. L. M., and Lage, J. L., 1996, ''Forced Convection in a Fluid-Saturated Porous-Medium Channel With Isothermal or Isoflux Boundaries,'' J. Fluid Mech., **322**, pp. 201–214.
[11] Sung, H. J., Kim, S. Y., and Hyun, J. M., 1995, ''Forced Convection From an Isolated Heat Source in a Channel With Porous Medium,'' Int. J. Heat Fluid Flow, **16**, pp. 527–535.
[12] You, H. I., and Chang, C. H., 1997, ''Determination of Flow Properties in Non-Darcain Flow,'' ASME J. Heat Transfer, **119**, pp. 840–843.
[13] You, H. I., and Chang, C. H., 1997, ''Numerical Prediction of Heat Transfer Coefficient for a Pin-Fin Channel Flow,'' ASME J. Heat Transfer, **119**, pp. 840–843.
[14] Neale, G., and Nader, W., 1974, ''Practical Significance of Brinkman's Extension of Darcy's Law: Coupled Parallel Flows Within a Channel and a Bounding Porous Medium,'' Can. J. Chem. Eng., **52**, pp. 475–478.
[15] Poulikakos, D., and Kazmierczak, M., 1987, ''Forced Convection in a Duct Partially Filled With a Porous Material,'' ASME J. Heat Transfer, **109**, pp. 653–662.
[16] Kim, S. Y., Kang, B. H., and Hyun, J. M., 1994, ''Heat Transfer From Pulsating Flow in a Channel Filled With Porous Media,'' Int. J. Heat Mass Transf., **37**, pp. 2025–2033.
[17] Chen, S. C., and Vafai, K., 1996, ''Analysis of Free Surface Momentum and Energy Transport in Porous Media,'' Numer. Heat Transfer, Part A, **29**, pp. 281–296.
[18] Nakayama, A., Kokudai, T., and Koyama, H., 1990, ''Non-Darcian Boundary Layer Flow and Forced Convection Heat Transfer Over a Flat Plate in a Fluid-Saturated Porous Medium,'' ASME J. Heat Transfer, **112**, pp. 157–162.
[19] Hong, J. T., Tien, C. L., and Kaviany, M., 1985, ''Non-Darcain Effects on Vertical-Plate Natural Convection in Porous Media With High Porosities,'' Int. J. Heat Mass Transf., **28**, pp. 2149–2157.
[20] Kaviany, M., 1987, ''Boundary layer treatment of forced convection heat transfer from a semi-infinite flat plate embedded in porous media,'' ASME J. Heat Transfer, **109**, pp. 345–349.
[21] Kuznetsov, A. V., 1996, ''Analytical Investigation of the Fluid Flow in the Interface Region Between a Porous Medium and a Clear Fluid in Channels Partially Filled With a Porous Medium,'' Appl. Sci. Res., **56**, pp. 53–67.
[22] Lan, X. K., and Khodadadi, J. M., 1993, ''Fluid Flow and Heat Transfer Through a Porous Medium Channel With Permeable Walls,'' Int. J. Heat Mass Transf., **36**, pp. 2242–2245.
[23] Nakayama, A., Koyama, H., and Kuwahara, F., 1988, ''An Analysis on Forced Convection in a Channel Filled With a Brinkman-Darcy Porous Medium: Exact and Approximate Solutions,'' Wearme-und Stoffeubertragung, **23**, pp. 291–295.
[24] Ould-Amer, Y., Chikh, S., Bouhadef, K., and Lauriat, G., 1998, ''Forced Convection Cooling Enhancement by use of Porous Materials,'' Int. J. Heat Fluid Flow, **19**, pp. 251–258.
[25] Vafai, K., and Kim, S. J., 1995, discussion of ''Forced Convection in a Porous Channel With Localized Heat Sources,'' ASME J. Heat Transfer, **117**, pp. 1097–1098.
[26] Vafai, K., and Kim, S. J., 1995, ''On the Limitations of the Brinkman-Forchheimer-Extended Darcy Equation,'' Int. J. Heat Fluid Flow, **16**, pp. 11–15.

[27] Tien, C. L., and Vafai, K., 1989, ''Convective and Radiative Heat Transfer in Porous Media,'' Adv. Appl. Mech., **27**, pp. 225–282.
[28] Kaviany, M., 1995, *Principles of Heat Transfer in Porous Media*, 2nd Ed., Springer-Verlag, New York.
[29] Nield, D. A., and Bejan, A., 1995, *Convection in Porous Media*, 2nd Ed., Springer-Verlag, New York.
[30] Vafai, K., 1984, ''Convective Flow and Heat Transfer in Variable-Porosity Media,'' J. Fluid Mech., **147**, pp. 233–259.
[31] Vafai, K., 1986, ''Analysis of the Channeling Effect in Variable Porosity Media,'' ASME J. Energy Resour. Technol., **108**, pp. 131–139.
[32] Vafai, K., Alkire, R. L., and Tien, C. L., 1985, ''An Experimental Investigation of Heat Transfer in Variable Porosity Media,'' ASME J. Heat Transfer, **107**, pp. 642–647.
[33] Poulikakos, D., and Renken, K., 1987, ''Forced Convection in a Channel Filled With Porous Medium, Including the Effects of Flow Inertia, Variable Porosity, and Brinkman Friction,'' ASME J. Heat Transfer, **109**, pp. 880–888.
[34] Renken, K., and Poulikakos, D., 1988, ''Experiment and Analysis of Forced Convective Heat Transport in a Packed Bed of Spheres,'' Int. J. Heat Mass Transf., **25**, pp. 1399–1408.
[35] Hunt, M. L., and Tien, C. L., 1988, ''Effects of Thermal Dispersion on Forced Convection in Fibrous Media,'' Int. J. Heat Mass Transf., **31**, pp. 301–309.
[36] Hunt, M. L., and Tien, C. L., 1988, ''Non-Darcian Convection in Cylindrical Packed Beds,'' ASME J. Heat Transfer, **110**, pp. 378–384.
[37] Hsiao, S. W., Cheng, P., and Chen, C. K., 1992, ''Non-uniform Porosity and Thermal Dispersion Effects on Natural Convection About a Heated Horizontal Cylinder in an Enclosed Porous Medium,'' Int. J. Heat Mass Transf., **35**, pp. 3407–3418.
[38] Hong, J. T., Yamada, Y., and Tien, C. L., 1987, ''Effect of non-Darcian Non-Uniform Porosity on Vertical-Plate Natural Convection in Porous Media,'' ASME J. Heat Transfer, **109**, pp. 356–362.
[39] Chen, H., 1996, ''Technical Note: Non-Darcy Mixed Convection From a Horizontal Surface With Variable Surface Heat Flux in a Porous Medium,'' Numer. Heat Transfer, Part A, **30**, pp. 859–869.
[40] Chen, H., 1997, ''Non-Darcy Mixed Convection Over a Vertical Flat Plate in Porous Media With Variable Wall Heat Flux,'' Int. Commun. Heat Mass Transfer, **24**, pp. 427–437.
[41] Chen, H., 1997, ''Analysis of Non-Darcian Mixed Convection From Impermeable Horizontal Surface in Porous Media: The Entire Regime,'' Int. J. Heat Mass Transf., **40**, pp. 2993–2997.
[42] David, E., Lauriat, G., and Cheng, P., 1991, ''A Numerical Solution of Variable Porosity Effects on Natural Convection in a Packed-Sphere Cavity,'' ASME J. Heat Transfer, **113**, pp. 391–399.
[43] Hsu, T., and Cheng, P., 1990, ''Thermal Dispersion in a Porous Medium,'' Int. J. Heat Mass Transf., **33**, pp. 1587–1597.
[44] Cheng, P., Hsu, C. T., and Chowdary, A., 1988, ''Forced Convection in the Entrance Region of a Packed Channel With Asymmetric Heating,'' ASME J. Heat Transfer, **110**, pp. 946–954.
[45] Fu, W., Huang, H. C., and Liou, W. Y., 1996, ''Thermal Enhancement in Laminar Channel Flow With a Porous Block,'' Int. J. Heat Mass Transf., **39**, pp. 2165–2175.
[46] Chen, H., Chen, T. S., and Chen, C. K., 1996, ''Non-Darcy Mixed Convection Along Non-isothermal Vertical Surface in Porous Media,'' Int. J. Heat Mass Transf., **39**, pp. 1157–1164.
[47] Jang, J. Y., and Chen, J. L., 1992, ''Forced Convection in a Parallel Plate Channel Partially Filled With a High Porosity Medium,'' Int. Commun. Heat Mass Transfer, **19**, pp. 263–273.
[48] Hong, J. T., and Tien, C. L., 1987, ''Analysis of Thermal Dispersion Effect on Vertical-Plate Natural Convection in Porous Media,'' Int. J. Heat Mass Transf., **30**, pp. 143–150.
[49] Cheng, P., and Hsu, C. T., 1986, ''Fully-Developed, Forced Convective Flow Through an Annular Packed-Sphere Bed With Wall Effects,'' Int. J. Heat Mass Transf., **29**, pp. 1843–1853.
[50] Cheng, P., and Zhu, C. T., 1987, ''Effect of Radial Thermal Dispersion on Fully Developed Forced Convection in Cylindrical Packed Tubes,'' Int. J. Heat Mass Transf., **30**, pp. 2373–2383.
[51] Cheng, P., and Vortmeyer, D., 1988, ''Transverse Thermal Dispersion and Wall Channeling in a Packed Bed With Forced Convective Flow,'' Chem. Eng. Sci., **43**, pp. 2523–2532.
[52] Vafai, K., and A. Amiri, 1998, ''Non-Darcian Effects in Confined Forced Convective Flows.'' *Transport Phenomena in Porous Media*, D. B. Ingham and I. Pop, eds., Pergamon, England, pp. 313–329.
[53] Amiri, A., and Vafai, K., 1994, ''Analysis of Dispersion Effects and Non-thermal Equilibrium, Non-Darcian, Variable Porosity, Incompressible Flow Through Porous Media,'' Int. J. Heat Mass Transf., **37**, pp. 939–954.
[54] Amiri, A., Vafai, K., and Kuzay, T. M., 1995, ''Effects of Boundary Conditions on Non-Darcian Heat Transfer Through Porous Media and Experimental Comparisons,'' Numer. Heat Transfer, Part A, **27**, pp. 651–664.
[55] Amiri, A., and Vafai, K., 1998, ''Transient Analysis of Incompressible Flow Through a Packed Bed,'' Int. J. Heat Mass Transf., **41**, pp. 4259–4279.
[56] Hwang, G. J., Wu, C. C., and Chao, C. H., 1995, ''Investigation of Non-Darcian Forced Convection in an Asymmetrically Heated Sintered Porous Channel,'' ASME J. Heat Transfer, **117**, pp. 725–732.
[57] Dixon, A. G., and Cresswell, D. L., 1979, ''Theoretical Prediction of Effective Heat Transfer Parameters in Packed Beds,'' AIChE J., **25**, pp. 663–676.
[58] Kuznetsov, A. V., 1997a, ''Thermal Non-equilibrium, Non-Darcian Forced Convection in a Channel Filled With a Fluid Saturated Porous Medium–A Perturbation Solution,'' Appl. Sci. Res., **57**, pp. 119–131.
[59] Ergun, S., 1952, ''Fluid Flow Through Packed Columns,'' Chem. Eng. Prog., **48**, pp. 89–94.
[60] Benenati, R. F., and Brosilow, C. B., 1962, ''Void Fraction Distribution in Beds of Sphere,'' AIChE J., **8**, pp. 359–361.
[61] Lee, D. Y., and Vafai, K., 1999, ''Analytical Characterization and Conceptual Assessment of Solid and Fluid Temperature Differentials in Porous Media,'' Int. J. Heat Mass Transf., **42**, pp. 423–435.
[62] Kuznetsov, A. V., 1994, ''An Investigation of Wave of Temperature Difference Between Solid and Fluid Phases in a Porous Packed Bed,'' Int. J. Heat Mass Transf., **35**, pp. 3030–3033.
[63] Kuznetsov, A. V., 1997b, ''A Perturbation Solution for Heating a Rectangular Sensible Heat Storage Packed Bed With a Constant Temperature at the Walls,'' Int. J. Heat Mass Transf., **40**, pp. 1001–1006.
[64] Alazmi, B., and Vafai, K., 2000, ''Analysis of Fluid Flow and Heat Transfer Interfacial Conditions Between a Porous Medium and a Fluid Layer,'' Int. J. Heat Mass Transf., to appear.